Engineering Structures 180 (2019) 205–222

Contents lists available at ScienceDirect

Engineering Structures

journal homepage: www.elsevier.com/locate/engstruct

Impact assessment of a wind turbine blade root during an offshore mating process

Amrit Shankar Verma[a,b], Zhiyu Jiang[b,c,*], Nils Petter Vedvik[d], Zhen Gao[a,b,e], Zhengru Ren[a,b,e]

[a] Department of Marine Technology, Norwegian University of Science and Technology (NTNU), Norway
[b] Centre for Marine Operations in Virtual Environments (SFI MOVE), NTNU, Norway
[c] Department of Engineering Sciences, University of Adger, 4879 Grimstad, Norway
[d] Department of Mechanical and Industrial Engineering, NTNU, Norway
[e] Centre for Autonomous Marine Operations and Systems (SFF AMOS), NTNU, Norway

ARTICLE INFO

Keywords:
Offshore wind turbine blade
Mating phase
Jack-up vessel
Monopile
Impact loads
Wind excitations
T-bolt connections
Marine operations

ABSTRACT

Single-blade installation is a popular method for installing blades on bottom-fixed offshore wind turbines. A jack-up crane vessel is often employed, and individual blades with their roots equipped with mechanical joints and bolted connections are lifted to the tower-top height and mated with a pre-assembled hub. The final mating phase is challenging and faces significant risks of impact. Due to relative motions between the blade and the hub, substantial impact forces may arise and lead to severe structural damages at root connections, thereby causing delays in the installation task. The present paper considers a realistic scenario of the mating process and investigates the consequences of such impact loads. Here, a single-blade model with tugger lines and a monopile model were established using a multi-body formulation, and relative velocities under collinear wave and wind conditions were obtained. A three-dimensional finite element model was developed for the blade root with T-bolt connections, and an impact investigation was performed for the case in which a guiding connection impacts the hub. The results show severe bending and plastic deformation of the guide pin bolt together with failure of the adjoining composite laminate at the root connection. Based on the type of damage obtained for the different environmental conditions considered, this paper also discusses its consequence on the installation tasks and suggests onboard decision making in case of an impact incident. The results of this study provide new insights regarding the mating phase and can be utilised to establish response-based operational limits.

1. Introduction

The constant need for renewable sources of energy has increased the demand for wind turbines, both in the onshore and offshore sectors [1,2]. In addition, the favourable factors in the offshore environment, such as the distant location of turbines from human settlements, large space to deploy big turbines and the possibility to transport them on barges, make offshore turbines more attractive than land-based turbines. Consequently, the rated capacity of offshore wind turbines has increased at a rate of 102% over the past decade, with monopile-type offshore wind turbines accounting for more than 87% of the total installed turbines in the European market [3,4].

The recent report [5] from the European Wind Energy Association suggests that by 2050, offshore wind energy could exceed the total onshore wind energy capacity [5–7]. However, achieving this goal would require turbines with rated power capacities that are larger than those of the existing turbines to be installed in deeper waters and far away from the shore. Note that in the year 2017 alone, the average rated capacity of all the offshore wind turbines that are grid connected in European waters was 5.9 MW [4] along with turbines with rated capacities reaching 8 MW. The recently announced Haliade-X 12 MW class of offshore wind turbines by General Electric (GE) will have blades that are 107 m long and that are mounted at a hub height of approximately 260 m above the mean sea level [8]. One of the main objectives for this class of turbines is to reduce the number of turbine units in an offshore farm. This presents less outflow of the capital on the overall balance of the plant [8] and is expected to reduce the total installation time involved in commissioning a farm, making the offshore wind market more competitive.

Although the continuous increase in the size of the turbines is an efficient and economical choice from an operational perspective, it poses challenges and risks during the assembly and installation phases.

* Corresponding author at: Department of Engineering Sciences, University of Adger, 4879 Grimstad, Norway.
E-mail addresses: amrit.s.verma@ntnu.no (A.S. Verma), zhiyu.jiang@uia.no (Z. Jiang), nils.p.vedvik@ntnu.no (N.P. Vedvik), zhen.gao@ntnu.no (Z. Gao), zhengru.ren@ntnu.no (Z. Ren).

https://doi.org/10.1016/j.engstruct.2018.11.012
Received 15 May 2018; Received in revised form 18 October 2018; Accepted 5 November 2018

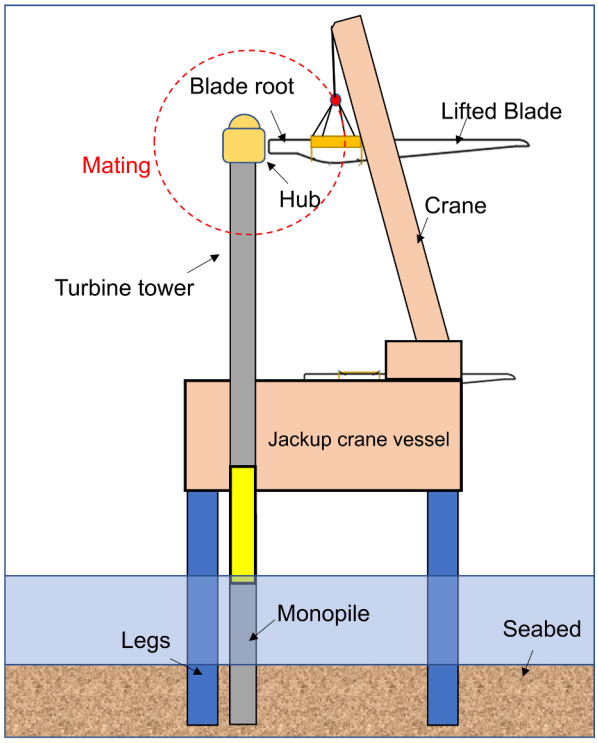

Fig. 1. Mating phase of the blade installation.

The components of wind turbines, particularly the blades and nacelle, are extremely sensitive and require high precision during transportation and installation in the offshore environment [2,9,10]. This high accuracy requirement makes the installation phase even more challenging with larger blades, power electronics and gearbox in nacelle [11]. In current practice, various methods for the assembly and installation of the turbines exist, among which the split-type installation method is the most popular for installing monopile-type offshore wind turbines [12]. Under this method, all the components of the turbines are individually lifted and assembled offshore, thus enabling the lifting operation to be performed with a crane that has less lift capacity. Additionally, higher deck usage is utilised during the transportation phase with individual unassembled components stacked on the vessel, thereby significantly reducing the overall transportation time. All these factors make the split-type installation method highly preferred. A jack-up crane vessel (Fig. 1) is often used as the installation vessel during the assembly and installation of wind turbine generator (WTG) components, which include blades, tower, nacelle, and hub [11]. These crane vessels can be utilised in shallower waters up to depths of 30–50 m, and they have legs that are jacked up during the installation phase with the legs anchored into the seabed [11] (Fig. 1). This makes the vessel and the object being lifted free from wave excitations to a large extent during the lifting operation, thus providing a stable platform.

Nevertheless, despite the stable installation system offered by jack-up crane vessels, single-blade installation on a monopile-type offshore wind turbine is still one of the most critical and challenging methods [12,14]. Significant relative motions between the blade root and the hub manifest during their alignment phase prior to being mated together [12], and these motions pose a significant risk of impact of the blade root with the hub (Fig. 2). Recently, there have been several incidents reported in the industry that include such impacts during mating [15]. There are several factors contributing to the relative motions between these components causing such impacts. Wind turbine rotor blades are aerodynamically shaped wide and long structures, and during the mating phase at a very high hub height, wind-induced forces produce pendulum oscillation motions at the blade root. Moreover, the

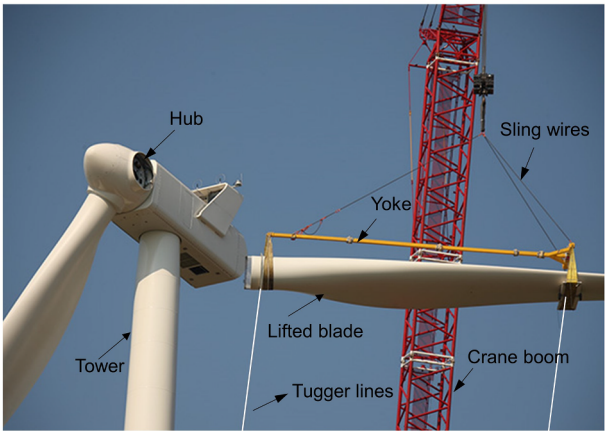

Fig. 2. Image of a wind turbine blade being prepared to mate with hub of a turbine (source: [13]).

large motion of the hub at the tower top, primarily developed because of the wave-induced loads on the monopile structures [12,14], makes the mating process even more challenging. In general, a monopile foundation structure acts as a cantilever beam with one end fixed into the seabed and possesses limited structural, soil, and hydrodynamic damping with an overall damping ratio in the first aft mode of approximately 1% [12]. Thus, any lifting operation in a wave excitation nearing the natural period of a monopile could trigger a resonance-driven high-oscillation motion in the pre-assembled hub. Moreover, the limitation of a jack-up crane vessel to shelter the monopile from wave loads during the installation phase (as the legs are jacked up) makes the mating process even more critical. Overall, there could be large relative motions developed between the blade root and hub during the mating phase [14]. Consequently, substantial impact forces are anticipated at the blade root in the case of an accidental impact and could damage the blade root locally. Such accidental events on the blade root could still have very high consequences on the blade's structural integrity because the root section of a blade resists the maximum flapwise and edgewise moments and torques developed in the blade during its design life [16]. Thus, the severity of such accidental impacts at the blade root during the mating process is a question of utmost concern. Additionally, any damage to the root connection during mating would require the lifted blade to be brought back onto the vessel, causing perplexity among the offshore crew regarding the decision to repair, replace or continue with another trial of mating the blade with the hub. A delay in the overall installation operation is therefore inevitable, causing loss of favourable weather windows, and is thus crucial for investigation. The present paper focuses on the impact assessment of the blade root during such accidents, and based on the type of damage obtained, it discusses the consequences on the installation tasks and suggests onboard decision making following the impact. This paper also briefly discusses the choice of favourable sea states for performing such mating processes.

To the authors' knowledge, there is still no published research on the impact assessment of a blade root in a scenario wherein it is being mated with the hub. This paper is expected to contribute to better planning of such offshore operations and develop guidelines that could aid the offshore crew in reacting to such accidental events. This would reduce the installation cost, quantify the risks involved during the critical mating operation and create confidence to match the industry's demand for installing larger turbines in the future. The remainder of this paper is organised in the following manner. Section 2 describes the problem statement, possible contact scenarios and numerical approach considered for the impact assessment in this paper. Section 3 describes the modelling of the installation system representing the mating operation and the environmental conditions considered for the study. Section 4 describes the structural impact modelling of the blade root

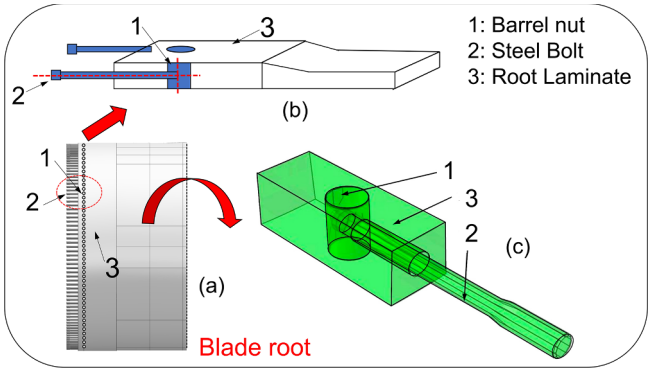

Fig. 3. (a) A typical wind turbine blade root with mechanical connections. (b) Zoom in view of blade root showing T-bolt connection. (c) Components of a typical T-bolt connection [19].

with the hub along with the constitutive material model implemented for the failure estimate at the blade root. Section 5 presents the results and discusses the relative motions developed between the root and the hub, followed by the description of failure at the blade root. Section 6 concludes the paper and finally Section 7 presents the limitation and future work.

2. Problem statement and numerical approach

A wind turbine blade is designed to be attached to the pitch bearing and the hub of a turbine through mechanical joints and connections at its root (Fig. 3(a)) [17,18]. In current practice, different types of blade root connections exist for this purpose, including T-bolt-type connections, flange-type connections, and carrot- or stud-type root connections [17]. Among all these connections, the T-bolt-type connection, due to its low cost, ease of manufacturing and high reproducibility features, is the most popular. The present study considers the T-bolt-type root connection for impact investigation [20,21,19] (Fig. 3). These connections are uniformly spread along the circumference of the blade root and are placed after the blade manufacturing process is completed. Each T-bolt connection at the blade root (Fig. 3(b), (c)) consists of a steel barrel nut and a steel bolt [22] fitted together into the thick composite laminate at the root. A barrel nut is a cylindrical component made of steel and is fitted into a through-the-plane hole made in the root laminate at the blade root section. The barrel nut is then joined with the surface of the laminate hole through an adhesive, and it is kept at a specific distance from the edge of the blade root [19]. The steel bolt is screwed into the barrel nut and is placed in the root through an in-plane hole drilled in the laminate (Fig. 3). The transfer of the operational loads from the blade root to the hub through these connections relies on the pre-tension of the bolt, normal stresses [18] and contact between the barrel nut and adjoining laminates.

In addition to these load-carrying structural connections, a few guiding connections [23] are also present at the blade root (Fig. 4). These connections are also configured in the blade as T-bolt connections; however, they have comparatively longer bolts, generally called ‘guide pins’ (Fig. 4). These longer bolts make it possible for an offshore banksman located inside the hub to visually monitor the blade root motion (Fig. 4(a)) with respect to the annular holes in the hub (Fig. 4(b)) and thus aid in the mating process. During the alignment phase, these guiding connections are the first to approach the hub during mating and are thus the most likely to be exposed to an accidental impact prior to other T-bolt connections at the blade root. The present paper considers a case in which a guiding connection with a guide pin at the blade root impacts the hub.

Moreover, it is the relative motion between the root and hub during the mating process that decides the possible impact scenarios whereby a blade root impacts the hub (Fig. 5). The first impact scenario includes a head-on impact between the blade root and hub arising due to the relative motion developed along the longitudinal axis of the lifted blade (Fig. 5). This enforces impact between the hub and the guide pin bolts of the root connections in its axial direction and is likely to be less critical. This is because the bolts are designed primarily to handle axial loads during normal operations, and thus, an impact in this direction is expected to be less severe.

The other impact scenario is a sideways impact between the root and hub developed due to relative motions in the lateral direction of the lifted blade (Fig. 5). This causes transverse impact forces on the guide pin bolts, which could damage the bolts and the adjoining laminate at the root connection. This is considered to be a critical scenario from a structural perspective because any damage to the composite laminates at the root is complex, cannot always be visually detected and could still severely affect the blade’s ultimate and fatigue strengths [10]. The study in this paper considers the latter contact scenario for impact investigation, which will be addressed in the following sections.

The velocity and the forces with which the blade root impacts the hub for a particular scenario depend on their relative motions. Hence, to perform an impact assessment, it is imperative to calculate the dynamic responses in the installation system developed during an offshore mating process in a particular sea state. Thus, this study also describes the modelling of the global installation system describing the mating process. A complete overview of the entire approach and the analysis procedure applied in this study is presented in Fig. 6. First, the installation system representing the mating process and consisting of two sub-systems (pre-assembled monopile and single blade) is numerically modelled in HAWC2. The first sub-system (sub-system 1) accounts for the hydrodynamic and soil models for the monopile and wind drag loads on the tower, nacelle and hub while the other sub-system (sub-system 2) accounts for the aeroelasticity of the blade during lifting. Then, time-domain simulations are conducted for wave and wind conditions, and the relative velocity between the blade root and hub is analysed. Second, the blade along with the T-bolt connection at its root and the hub are modelled using the finite element method, and the impact investigation is performed using Abaqus Explicit. The modelling technique considers the three-dimensional stresses at the root connection along with a contact non-linear formulation and the entire inertia of the blade for impact investigation. Then, the damages occurring at the blade root for different impact velocities corresponding to different sea states are analysed. Finally, based on the type of damage obtained, the consequence on the installation activity after impact and discussions on the choice of a favourable sea state for mating operations are presented.

3. Modelling of the global installation system

HAWC2 was used to model the global installation system. HAWC2 is an aeroelastic code developed by the Technical University of Denmark [24]. This code is based on multi-body dynamics and has been widely used for dynamic response analysis of wind turbine systems in the time domain. It has modelling capabilities to account for structural dynamics while considering external effects, loads and control systems. The structures constituting the installation system are divided into a number of independent objects in HAWC2, with each body modelled as Timoshenko beam elements. The bodies are connected to each other through couplings.

A jack-up crane vessel, a lifting system, and a pre-assembled monopile are involved. The global installation system provides a simplified representation of the physical system, which is used for estimating the relative motions between the blade root and the hub. It is assumed that both the jack-up vessel and crane are rigid and jack-up is rigidly fixed to the seabed with pile-soil interaction for its legs ignored. In this way, the jack-up crane vessel is not explicitly modelled, and the crane tip is simplified as a fixed boundary condition. This simplification is also adopted in [14,25], as proprietary information of the jack-up

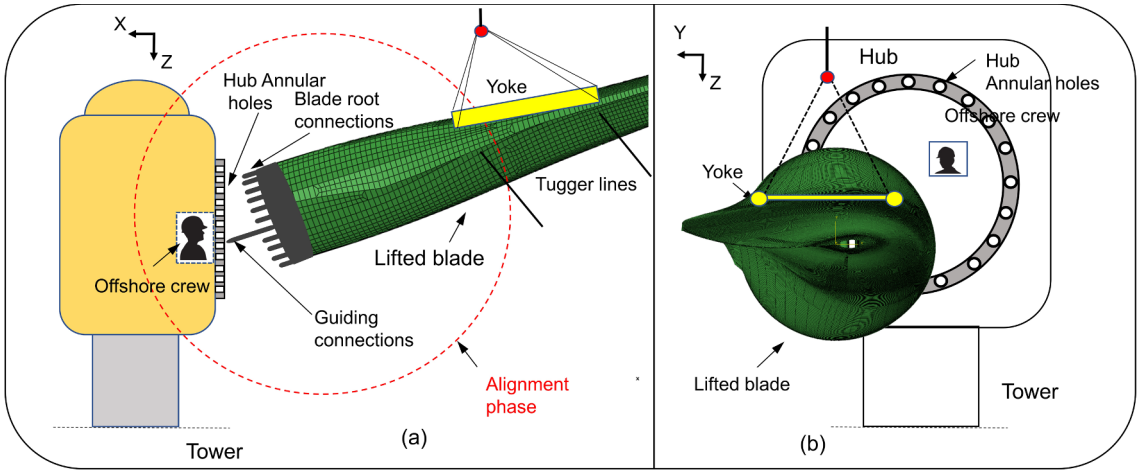

Fig. 4. Guiding connection at the blade root (a) Alignment phase. (b) Annular holes in the hub.

crane vessel is not available. The global installation system includes two sub-systems (Fig. 7): (1) a pre-assembled monopile system and (2) a single-blade system. These sub-systems along with their modelling details and the basis for their response evaluation are discussed in the following.

3.1. Pre-assembled monopile system

The first sub-system consisted of a pre-assembled monopile foundation, a tower, a nacelle, and three hubs (Fig. 7). The monopile support structure for the DTU 10 MW wind turbine utilised in this study is designed by Velarde (2016) [26] and has a diameter of 9 m with a pile penetration depth of 45 m. Assuming the soil properties of a uniform sand layer, Velarde [26] extracted the lateral stiffness of the soil represented by *p-y* curves from finite element analysis. In HAWC2, the monopile foundation is modelled by Timoshenko beam elements, and the soil effect is represented by distributed springs, which idealises the pile as a free-free beam with lateral springs distributed along the adjoining soil portions; see Fig. 7. The damping ratios of the first fore-aft and side-side modes of the monopile system were tuned to be approximately 1%, which is consistent with the experiments on monopile foundations [27,28]. Moreover, the tower, nacelle, and hubs used in this sub-system were based on the DTU 10 MW reference wind turbine [29], and these structural components were also modelled in HAWC2. The characteristics of the different components of the pre-assembled monopile system are listed in Table 1.

There are hydrodynamic loads acting on the monopile structure. In HAWC2, the hydrodynamic loads are evaluated by Morison's equation [30,31], which is applicable to slender structures. The hydrodynamic force per unit length normal to each strip is expressed as:

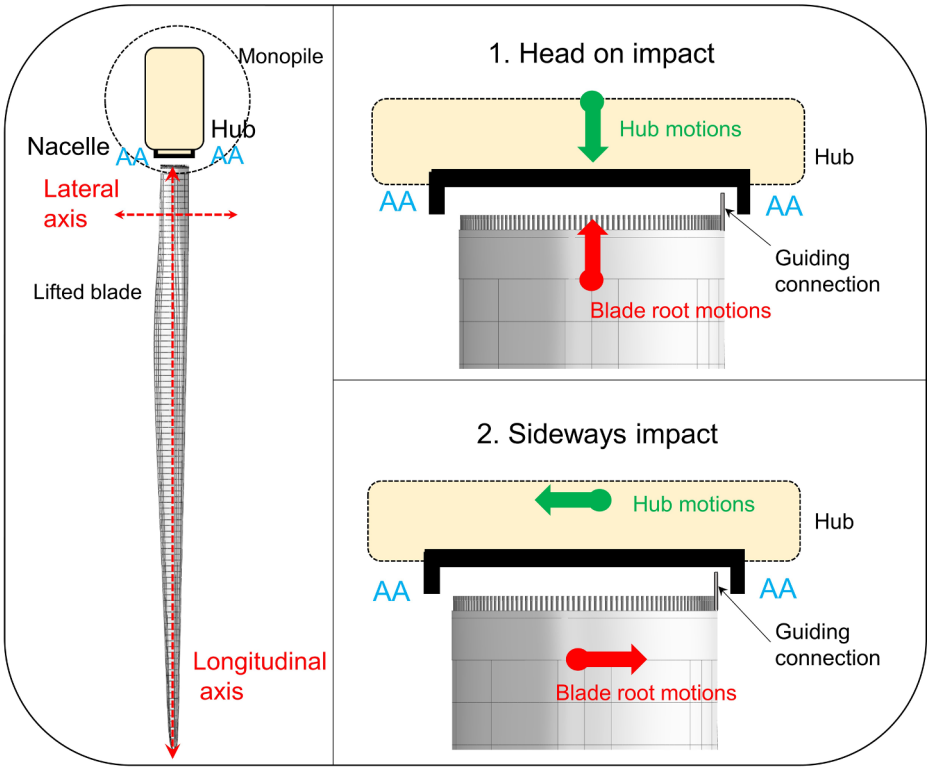

Fig. 5. Impact scenarios during mating.

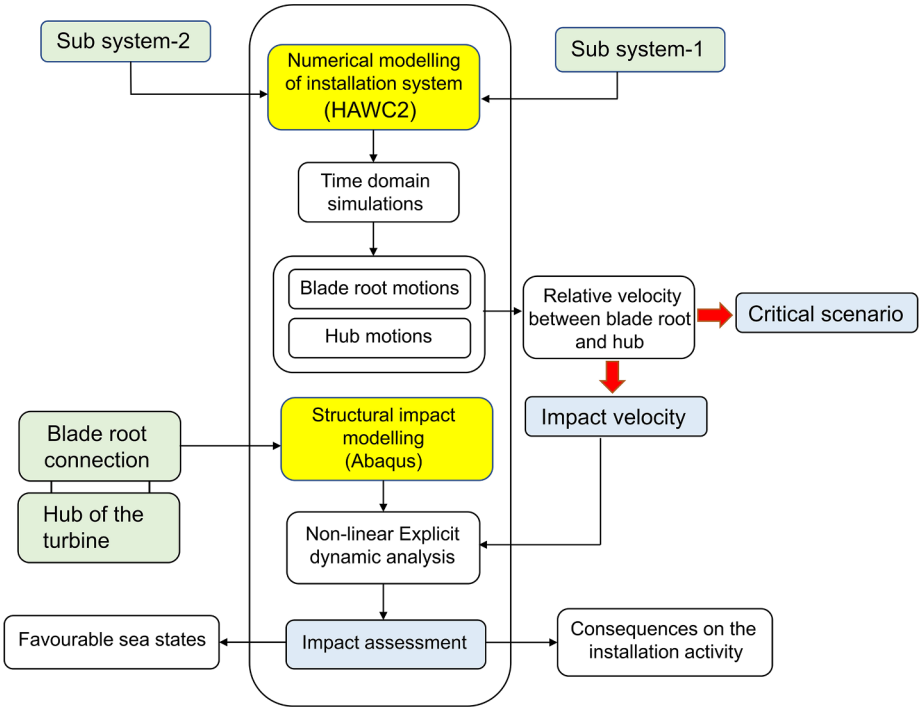

Fig. 6. An overview of the numerical approach applied in the study.

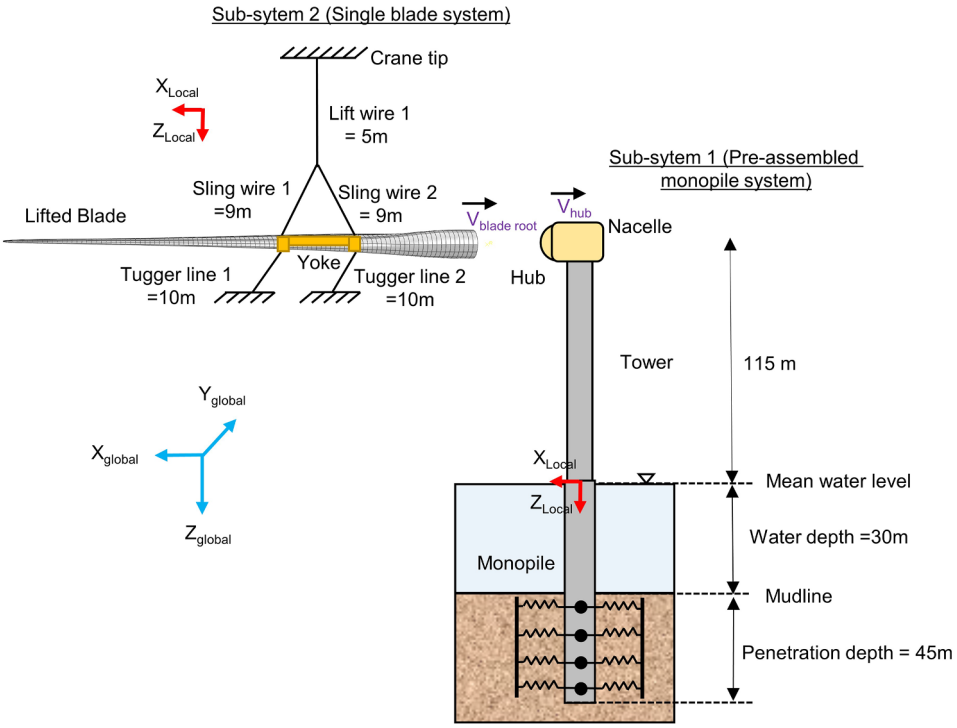

Fig. 7. Modelling of the global installation system and its sub-sytems.

$$f_s = \rho C_M \frac{\pi D^2}{4}\ddot{x_w} - \rho(C_M - 1)\frac{\pi D^2}{4}\ddot{\eta_1} + \frac{1}{2}\rho C_D D(\dot{x_w} - \dot{\eta_1})|\dot{x_w} - \dot{\eta_1}|, \quad (1)$$

where ρ is the density of sea water, taken as 1029 kg/m^3; $D$is the monopile diameter, taken as 9 m; C_M is the mass coefficient, assumed as 2 in this study; and C_D is the drag coefficient, taken as 1. Furthermore, $\dot{x_w}$ and $\ddot{x_w}$ are the velocity and acceleration, respectively, of water particles at the centre of the strip, and $\dot{\eta_1}$ and $\ddot{\eta_1}$ are the velocity and acceleration, respectively, of the monopile foundations. Morison's equation consists of drag and inertial terms, of which the inertial term is dominant [12,14]. The Morison's equation is suitable for calculating hydrodynamic loads on the monopile structure when the ratio between the wave length and monopile diameter (D) is greater than 5. For a ratio less than 5, potential flow theory should be used to calculate wave-induced loads [32]. However, the application of potential theory will be computationally demanding in time-domain simulations. For simplicity, a constant C_m of 2.0 was applied, which can be on the conservative side with respect to the motions of the monopile.

Table 1
Characteristics of different components.

S. No	Parameter	Value
1	Monopile diameter (m)	9
2	Monopile penetration (m)	45
3	Natural period of the 1st fore-aft mode (s)	4.2
4	Damping ratio of the 1st fore-aft mode	1%
5	Blade mass (ton)	41.7
6	Yoke mass (ton)	50
7	Tugger line mass per unit length (kg/m)	306
8	1st rotational mode of the blade about the global y-axis (Hz)	0.08

3.2. Single-blade system

The second sub-system modelled in HAWC2 consists of an 86.4 m long DTU 10-MW blade [29] lifted by a yoke and attached with two tugger lines along with lift and sling wires connected to a fixed crane tip (Fig. 7). These tugger lines are generally used to constrain the blade motion in the horizontal plane, with their attachment points in the model placed at an equal distance to the blade's centre of gravity. Each tugger line was 10 m long, consisting of cables, each of length 1 m and were linked to each other by spherical joints, which further makes it possible for the tugger lines to exhibit non-compressible behaviour during mating. Additionally, one end of each tugger line and the lift wire were connected to the crane. The blade was modelled as one single body, and the leading edge of the blade was oriented perpendicular to the direction of the wind (zero degree pitch angle).

Furthermore, for evaluating the blade root motions due to turbulent wind field, Mann's turbulence box [33] in HAWC2 was utilised. This turbulence box is based on Mann's turbulence model and follows the isotropic turbulence in neutral atmospheric situations. The model also considers the effect of non-isotropic turbulence by applying rapid distortion theory [33]. Since the lifted blade is assumed to be in steady state and is non-rotating during the mating phase at the hub height, steady aerodynamic lift and drag coefficients were utilised to estimate the wind loads on each section of the blade. Here, the cross-flow principle [34] was utilised in the HAWC2 code, which considers the wind flow to be two dimensional (2D) and neglects the component of the wind in the spanwise direction of the blade.

3.3. Load cases

To estimate the relative motions between the blade root and hub during the mating phase and to later consider a scenario in which the blade root impacts the hub, the environmental conditions (EC) representing the mating operation in a relatively rough sea state were analysed. Moreover, the paper considered all the load cases with collinear wind and wave conditions (Fig. 8(a)). A load case (EC-I) was also considered where the mating operation was assumed to be performed in a sea state with a wave spectral peak period (T_P) close to 4 s, which approaches the first fore-aft natural period of the monopile. This is expected to provide very high hub motions at the tower top and is critical to study (Fig. 8(a)). Additionally, the mean wind speed (U_W) considered in this paper was taken as 10 m/s at the hub height, which is regarded as an acceptable wind condition for blade installation in industry [9]. A value of 0.12 was taken as the turbulence intensity (T_I), which is for a given U_W and for a particular turbine class obtained from the IEC 61400-1 [35] guidelines. Table 2 lists all the load cases utilised in this paper, where EC in the table stands for environmental conditions, H_S stands for significant wave height, T_P stands for spectral peak period, U_W stands for mean wind speed, and T_I stands for turbulence intensity. The irregular waves in this study were generated using the JONSWAP spectrum [36]. Finally, time-domain simulations for dynamic response analyses were performed with a time step increment of 0.01 s. For each case of environmental conditions listed in Table 2, five 30-min (1800 s) simulations with random wave and wind seeds were performed to reduce statistical uncertainties, and the motions of the blade root and the hub were obtained. Parameters such as the time step increment and number of seeds for the analysis are chosen based on a sensitivity study. Further, each simulation lasted 2200 s, and the initial 400 s were discarded in the post-processing to neglect any transient effects. Here, an average of five seeds for each load case, with each seed evaluated for 30-min 90% fractile extreme value, was used for estimating the maximum relative velocity between the root and hub. This value is utilised as the reference velocity for the impact analysis and was assumed to be conservative. It was also assumed that the inertia of the monopile system is substantially larger than that of the blade system and that the motion of the hub is not affected by the blade impact. Hence, the relative velocity between the blade root and the hub evaluated from the HAWC2 code is suitable for the impact investigation in Abaqus. This is also addressed in Section 5, where the displacement and acceleration of the hub motion with and without the blade impact are presented and discussed.

4. Structural modelling of the guiding connection at the blade root

After the dynamic response analyses were performed based on the modelled installation system, finite element structural modelling of the blade root connection was required to investigate the consequence of its impact with the hub during mating. In this study, we consider the impact of a single guiding connection at the blade root, given that these guiding connections (Fig. 9) are the first to suffer impact with the hub during mating. The choice of studying the impact of a single guiding connection is conservative, as this assumption implicitly neglects any load distribution to the adjacent bolts during the impact event. Although it is likely that several bolts are involved in the impact, this conservative approach renders the assumption most relevant according to the objective of this study. A guiding connection at the blade root is principally a T-bolt connection, which has a barrel nut and a longer steel bolt (guide pin) fitted into the blade root laminate through in-plane and through-the-plane holes. Therefore, modelling such a connection requires the development of a three-dimensional finite element model that includes all these components with the implementation of a contact non-linear formulation. The modelling details are explained below.

4.1. Numerical modelling method and impact formulation

The three-dimensional finite element modelling and analyses in this study were performed using the Abaqus Explicit environment, a commercial finite element software developed by Dassault Systèmes Simulia Corp [38]. The explicit-based algorithm was chosen due to its capability to perform better than the implicit code while handling problems involving complex interactions, large rotations, and large deformations [39]. Hence, it was utilised for our case where we consider the blade root impacting the hub, which involves complex interactions. The algorithm further utilises the central difference operator and elements with a lumped mass matrix formulation [38], where the kinetic state and the dynamic equilibrium are satisfied at each time increment based on the solution known from the previous time increment. Nevertheless, the algorithm is conditionally stable [38], requiring a time increment for stress wave propagation that is less than a minimum stable time increment and is estimated automatically by the solver. However, the algorithm requires a sound check of energy history after the analysis to validate the numerical model's stability and suitability. We developed the three-dimensional model of the guiding connection at the blade root and the hub for impact investigation by utilising the modelling capabilities in Abaqus CAE (Computer-Aided Engineering) along with its scripting interface capabilities, the specifics of which are discussed below.

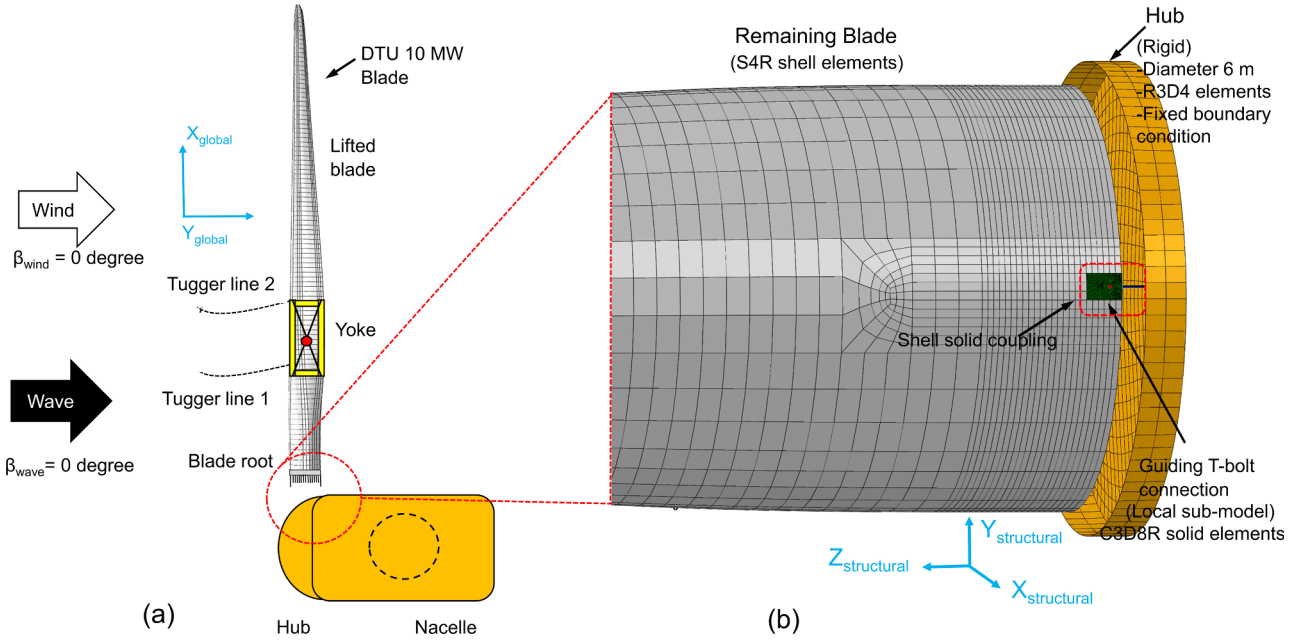

Fig. 8. (a) Illustration of the environmental conditions. (b) Finite element modelling of guiding connection at the blade root (rotated view with ninety degree with respect to (a)).

Table 2
Environmental conditions (wave-wind aligned).

EC	H_s (m)	T_p (s)	U_w (m/s)	TI
I	2	4	10	0.12
II	2	6	10	0.12
III	2	8	10	0.12
IV	2	10	10	0.12

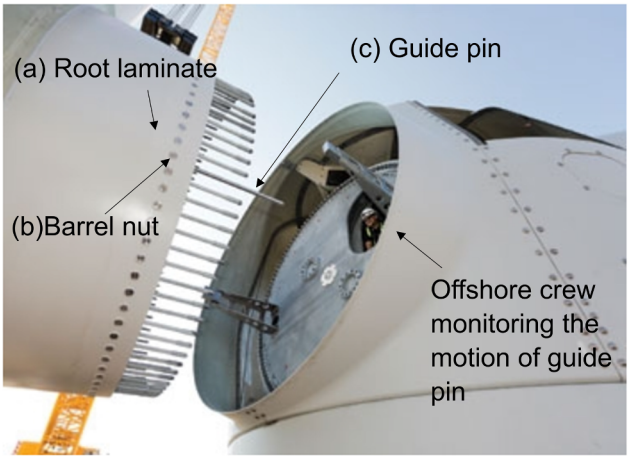

Fig. 9. Components of guiding connection of the blade root observed from a real time mating operation [37].

The base structural model utilised in this study was the DTU 10 MW reference wind turbine blade [29], where all the information including its finite element model, material properties and layup were obtained from their repository website *dtu-10mw-rwt.vindenergi.dtu.dk*. The blade is 86.4 m long and has a root diameter of 5.4 m, with its external and internal geometries originally discretised with shell elements. The main purpose of the blade was to investigate upscaling effects of blade length (from 5 MW to 10 MW) on its ultimate strength performance. Hence, the original model derived from the DTU repository had no explicit connection modelled at the root or any region in the blade and was defined with smeared properties. However, for the present study, the guiding connection at the blade root for the DTU 10 MW blade was required and was thus designed and developed separately with three-dimensional solid elements. This will be referred to in this study as a 'local sub-model' (Fig. 8(b), Fig. 10), and the name 'sub-model' must not be confused with the sub-modelling technique in Abaqus, where the solution of a local model is derived from a global coarser model.

The local sub-model consisted of (1) composite root laminate (represented by green colour in Figs. 10 and 11) with a thickness of 100 mm and had an in-plane hole (P) and through-the-plane hole (Q), (2) steel barrel nut with a diameter (ϕ_D) of 56 mm (represented by red colour), and (3) steel bolt (guide pin) with a nominal diameter (ϕ_d) of 28 mm and length (L) of 400 mm. The dimensions of these components of the guiding connections are based on the practice in industry [19,20], which were further validated based on a static strength design check for maximum flapwise and edgewise bending moments developed at the root section of the DTU 10 MW blade for extreme design loads [16,29,40]. In addition, the developed local sub-model was connected with the remaining structural shell model (represented by grey colour in Fig. 8(b) and Fig. 11) at its root, with a set of distributed coupling constraint equations (represented by red dots, Fig. 11), by utilising the 'shell to solid coupling' method available in Abaqus [38].

This shell to solid coupling feature enables the local detailed 3D model to be kinematically coupled to a coarser shell element region [38]. This is required to account for computational efficiency, where the analysis can be performed on elements considering three-dimensional stresses, while the entire blade discretised with coarser shell elements could provide the inertial effects to capture the true dynamics of the problem involving impact.

Furthermore, to model the root laminate and assign material properties to it, the information of the stacking sequence of the composite plies at the root region is required. The details of the layup at the blade root are generally confined to the industry's specific knowledge [40], and limited information is available in the literature published to date. Moreover, the DTU 10 MW blade is a non-existent blade and does not have a root-specific layup plan. The blade had shear webs extended until its root with a few regions even fused with balsa, which is not characteristic of a practical existing blade root used in industry. Consequently, the layup available from the parent definition was not

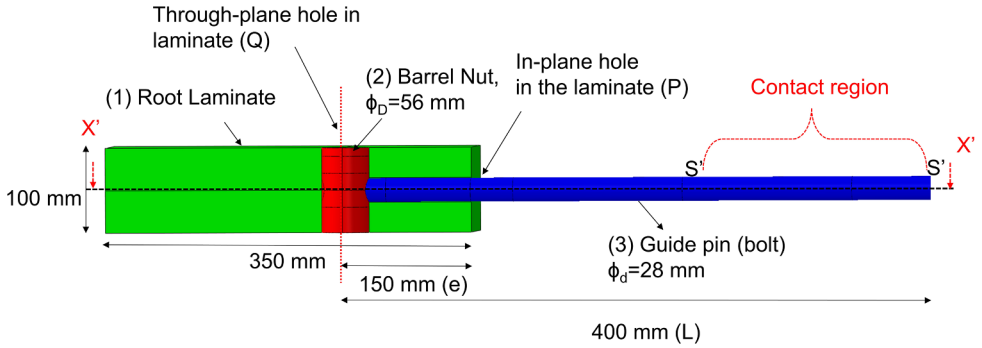

Fig. 10. Dimensions and components of the local sub-model.

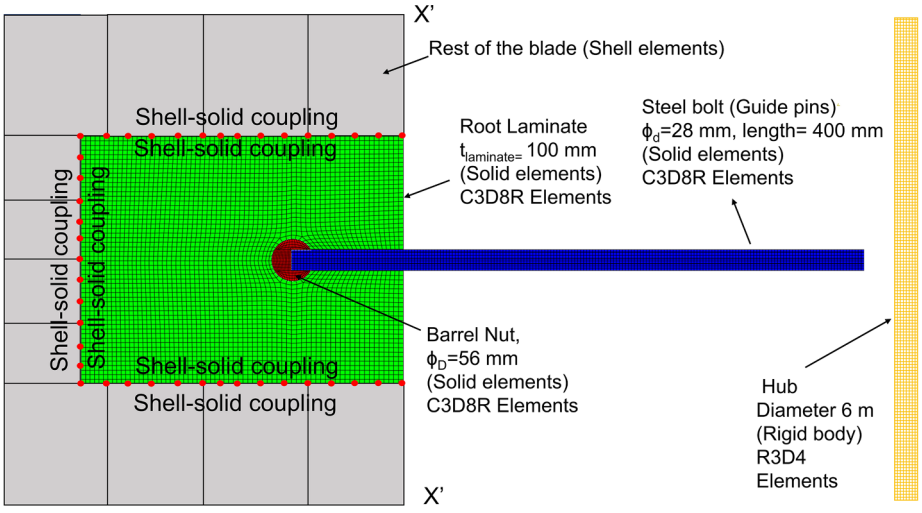

Fig. 11. Shell to solid coupling of the local sub-model with the blade root (X′X′).

utilised in this study for modelling the laminate at the local sub-model. Generally, a laminate at the root is kept conservatively thicker compared to other regions in the blade and is designed with either quasi-isotropic laminates having plies oriented in a [0/+45/−45/90] layup or with a triaxial-type layup with [0/+45/−45] plies [19]. In this study, the layup in the form of [0/+45/−45] was considered as the principal layup for the root laminate due to the availability of material properties obtained from [41]. These material properties correspond to the inputs from a blade manufacturer and were thus considered suitable.

The local sub-model at the blade root was defined with a [0/+45/−45] stacking layup plan and had a thickness of 100 mm. The composite laminate was modelled as a homogeneous orthotropic material, with elastic mechanical properties of the laminate derived based on the homogenisation principle [20,42]. Such an approach simplifies the modelling of laminates at the root, which in reality would have hundreds of layers of composite plies and would be an enormous computational expense if all the layers are modelled individually with solid elements [42]. The homogenisation principle is based on uniform linear displacement fields and computes the stiffness matrix of the homogenised laminate as the weighted average of the individual properties of the chosen principal layup. This approach enables predicting any failure state in the composites based on a maximum stress failure criterion. However, any distinct failure mode in the laminate, such as matrix cracking, fibre kinking or any delamination between the plies, cannot be explicitly modelled. Nevertheless, the work on progressive modelling of these failure modes at the blade root due to impact is a question of ongoing research and is beyond the scope of this paper. Furthermore, the threads at the guide pin bolt were neglected in this study, with one end of the guide pin (head) being inserted into the barrel nut and were together tie constrained. The tie constraint in Abaqus is a feature that enables a rigid fixity between the barrel nut and the guide pin head without any threaded connections. The guide pin head tied into the barrel nut enters through the in-plane hole of the laminate. The in-plane hole had a diameter of 29 mm and was kept slightly larger than the nominal diameter of the guide pin bolt as is practiced in industry and initially does not have any contact with the bolt. The contact interaction was still defined between them to model any possible contact during the impact event with the hub that can induce failure stresses in the laminate. Again, the barrel nut was appended into the through-the-plane hole at the root laminate, with contact defined under the general contact algorithm available in Abaqus Explicit along with a hard contact pressure over-closure interaction and frictionless behaviour. This was assumed to be suitable in this study because the adhesive that connects the barrel nut with the laminate in reality has a very limited structural stiffness and is only used to keep the barrel nut in position in the laminate hole [19].

The hub, with which the impact of the guiding connection is considered in this study, had a diameter of 6 m and was modelled (represented by yellow[1] colour, Fig. 8 (b) and Fig. 11) as a rigid body with a general structural representation and was discretised with 4-node, bilinear quadrilateral rigid (R3D4) elements. It was further constrained in all degrees of freedom. The contact between the hub and the portion of the guide pin (S′S′) considered for impact in this study (Fig. 10) was defined as a part of a general contact algorithm, implemented with penalty enforcement and a hard contact pressure over-closure

[1] For interpretation of color in Figs. 8, 10, 11 and 17, the reader is referred to the web version of this article.

interaction behaviour. The tangential contact behaviour between the impacting surfaces were defined using the friction coefficient value of 0.3 and is taken from [43,44]. The value is typical for metal to metal, and metal to plastic [45,46] contact surfaces during the impact simulation. Since the relative sliding distances between surfaces involved in the contacts are small, the value of the friction coefficient is not expected to have any significant influence on the analysis results. Furthermore, no other equipment involved in the lifting–such as yoke, tugger lines or lifting wires–was considered in the finite element model. All the nodes along the blade root section were connected with a reference node defined at the centre of the root section by a kinematic coupling constraint. This constrains the motion of all the nodes at the blade root with the motion of the reference node in a given degree of freedom. Finally, the local sub-model had a refined area with solid brick elements of size 5.56 mm and was discretised with a total of 109 K C3D8R elements. The element size was chosen based on a mesh convergence study, and the details will be discussed in Section 5. The C3D8R elements are standard hexahedral continuum solid elements with eight nodes and reduced integration. The remainder of the blade was modelled with 4-node general-purpose thick shell elements (S4R elements) with interfacial shell elements, which were coupled with the solid submodel having a refined mesh of size 20 mm. The other regions of the blade had a coarser mesh because their major contribution in the analysis was to account only for inertial loads during the impact. Finally, these analyses were performed using the Abaqus/explicit algorithm, with an automatic stable time increment ranging 10e−7 s, and they were run on an HPC machine with a cluster of 2 nodes, taking approximately 34 h to complete 1 s, which is the total simulation time. Note that the impact velocity used in Abaqus/explicit for damage assessment is obtained based on multi-body simulations in HAWC2, where the blade is modelled with beam elements. Therefore, the global stiffness of the blade based on beam and shell/solid elements were compared. The mass distributions, centre of gravity, and eigen frequencies of both the blade models were compared and verified to be in close agreement. This implies that these models are comparable and thus suitable for the study.

4.2. Implemented constitutive material model

4.2.1. Maximum stress criterion

In this study, a maximum-stress-based criterion is considered for predicting failure in the composite laminate at the blade root. This criterion is one of the simplest and most widely utilised failure models for the composite laminate [47]; however, it does not consider interactions between stress components. Nevertheless, this criterion is considered appropriate for our case because the focus of the study here is to estimate failure loads in the composite laminate rather than progressive damage analysis of the composite. In addition, since the impact is not being considered directly between the hub and the thick laminate at the root, discrete layer modelling is avoided at this level of analysis. Here, the individual normal stresses in 1 (σ_{11}), 2 (σ_{22}) and 3 (σ_{33}) directions and the shear stresses in 1–2 (σ_{12}), 1–3 (σ_{13}) and 2–3 (σ_{23}) planes are compared with their corresponding maximum allowable strength values. The failure in the laminate is predicted when at least one component of the stresses computed from the analysis (post-processed in ABAQUS [38] by S_{ij}) exceeds the maximum allowable strength of the laminate in that particular stress state.

A parameter *failure index* (F_I) is defined here in the criterion to represent the state of the laminate, where a value of F_I equal to or greater than 1 implies failure in the laminate. Eq. (2) presents a mathematically modified form for the maximum stress criterion. The failure index (F_I) is defined as the maximum value obtained from the modulus of the failure index ($|F_I(S_{ij})|$) estimated for each stress state ($i = 1, 2, 3; j = 1, 2, 3$) and is expressed as:

$$F_I = max.\begin{cases} |F_I(S_{11})|;\ \text{where } F_I(S_{11}) = \left(\frac{\sigma_{11}}{X^T}\right) \text{ if } \sigma_{11} > 0 \text{ or } \left(\frac{\sigma_{11}}{X^C}\right) \text{ if } \sigma_{11} < 0 \\ |F_I(S_{22})|;\ \text{where } F_I(S_{22}) = \left(\frac{\sigma_{22}}{Y^T}\right) \text{ if } \sigma_{22} > 0 \text{ or } \left(\frac{\sigma_{22}}{Y^C}\right) \text{ if } \sigma_{22} < 0 \\ |F_I(S_{33})|;\ \text{where } F_I(S_{33}) = \left(\frac{\sigma_{33}}{Z^T}\right) \text{ if } \sigma_{33} > 0 \text{ or } \left(\frac{\sigma_{33}}{Z^C}\right) \text{ if } \sigma_{33} < 0 \\ |F_I(S_{12})|;\ \text{where } F_I(S_{12}) = \left(\frac{\sigma_{12}}{S_{12}^l}\right) \text{ if } \sigma_{12} > 0 \text{ or } \sigma_{12} < 0 \\ |F_I(S_{13})|;\ \text{where } F_I(S_{13}) = \left(\frac{\sigma_{13}}{S_{13}^l}\right) \text{ if } \sigma_{13} > 0 \text{ or } \sigma_{13} < 0 \\ |F_I(S_{23})|;\ \text{where } F_I(S_{23}) = \left(\frac{\sigma_{23}}{S_{23}^t}\right) \text{ if } \sigma_{23} > 0 \text{ or } \sigma_{23} < 0 \end{cases} \tag{2}$$

where $F_I(S_{ij})$ is the individual failure index expressed as the normalised stress exposure factor. These exposure factors are obtained for each stress state ($i = 1, 2, 3; j = 1, 2, 3$), where stresses obtained from the analyses are normalised with their corresponding strength values. The advantage of these stress exposure factors is that they explicitly state how many times the stress levels in the laminate have exceeded their allowable stresses. Any exposure factor lying in the range ($\forall : F_I(S_{ij}) \in (-\infty, -1] \cup [+1, \infty]$) suggests failure in the laminate in a particular stress state; otherwise, ($\forall : F_I(S_{ij}) \in (-1, 1)$) suggests that the stress levels have not been exceeded. Here, any negative values correspond to compressive stress exposure factors, while positive values correspond to tensile stresses. The details of the material parameters for the homogenised laminate used in this study, including the strength of the laminate, are presented in Table 3, where the subscript 'T' stands for tensile and the subscript 'C' stands for compressive. Here, the through-the-thickness strength (Z^T and Z^C) values were not reported in the literature and were thus assumed to be equal to the strength values of the corresponding unidirectional lamina used in the homogenisation.

4.2.2. von Mises criterion with equivalent plastic strain

The material utilised for the barrel nut and the guide pin bolt is a grade 8.8 steel. A generic von Mises criterion with equivalent plastic strain indicator [38] is utilised in this study for predicting any damage in these materials due to impact. The steel is modelled with plasticity behaviour along with an isotropic hardening model [38] that is used with the von Mises yield function. With this isotropic hardening model, the yield surface (σ_0) in the stress space will evolve uniformly as plastic deformation occurs [38]. The equivalent plastic strain (ϵ^{pl}) is then obtained by integrating the equivalent plastic strain rate ($\dot{\epsilon}^{pl}$) over the deformation history (0→t) and is expressed as:

$$\epsilon_{pl} = \int_0^t \left(\sqrt{(2/3)\dot{\epsilon}^{pl} : \dot{\epsilon}^{pl}}\right) dt, \tag{3}$$

This is obtained by post-processing the output variable PEEQ (plastic equivalent strain) in Abaqus. The data points required for defining this isotropic model, i.e. the true stress as a function of logarithmic plastic strain, were calibrated from the engineering stress-strain curve obtained from the literature for the grade 8.8 steel [48]. The engineering properties and mechanical strength of the steel material implemented in this work are also presented in Table 4 of this paper.

Table 3
Material properties implemented for the homogenised laminate.

Property	Symbol	Value	Units
Density	ρ	1864.0	kg/m^3
Young's Modulus	E_1; E_2; E_3	21.69; 14.67; 12.09	GPa
Shear Modulus	G_{12}; G_{23}; G_{13}	9.413; 4.53; 4.53	GPa
Poisson's Ratio	ν_{12}; ν_{13}; ν_{23}	0.478; 0.275; 0.3329	-
Longitudinal strength	X^T; X^C	472.06; 324.16	MPa
Transverse strength	Y^T; Y^C	127.1; 127.1	MPa
Through thickness strength	Z^T; Z^C	38.25; 114.7	MPa
Shear strength	S_{12}^l;S_{13}^l;S_{23}^t	99.25; 78.21; 39.51	MPa

Table 4
Material properties implemented for the steel.

Property	Value	Units
Density (ρ)	7850	kg/m^3
Young's modulus (E)	210	GPa
Poisson's ratio (ν)	0.3	–
Yield stress (σ_y)	640	MPa
Ultimate stress (σ_u)	800	MPa

5. Results and discussion

This section presents the results and discussion on the dynamic response analyses and response statistics evaluated for the installation system modelled in HAWC2. Furthermore, the results of the impact investigation between the guiding connection and the hub modelled in Abaqus are presented and discussed.

5.1. Hub motions

The responses in the hub motions depend on the hydrodynamic wave loads acting on the monopile structure. Fig. 12(a)-(c) present the time histories for the velocity of the hub centre in the global X, Y, and Z directions (V_x, V_y, and V_z) for the load case EC-I (H_s = 2 m, T_p = 4 s). These figures clearly show that the motion of the hub is substantially higher in the global Y direction (average of 5 seeds with 90% fractile maximum is 0.99 m/s, Fig. 12(b)) compared to its motion in the X and Z directions, where the velocity is significantly low (Fig. 12(a) and (c); maximum value of 0.0015 and 0.005 m/s, respectively). Similar observations are found for all other load cases (EC-II, III, and IV) considered in this study, where the motion of the hub in the global Y direction is found to be largely dominant. Consequently, this paper only considers the motion of the hub in the global Y direction to calculate the relative velocity between the blade root and hub because the major contribution is from the motion of the hub in this direction. The relative motion considered in the global Y direction would imply that the impact scenario would involve a sideways impact of the blade root with the hub, and this corresponds to the motion of the blade in the X direction of the blade finite element coordinate system in Abaqus. This confirms the objective of our impact assessment study, where sideways impact with the hub was critical.

Fig. 13 presents the comparison between the velocity of the hub

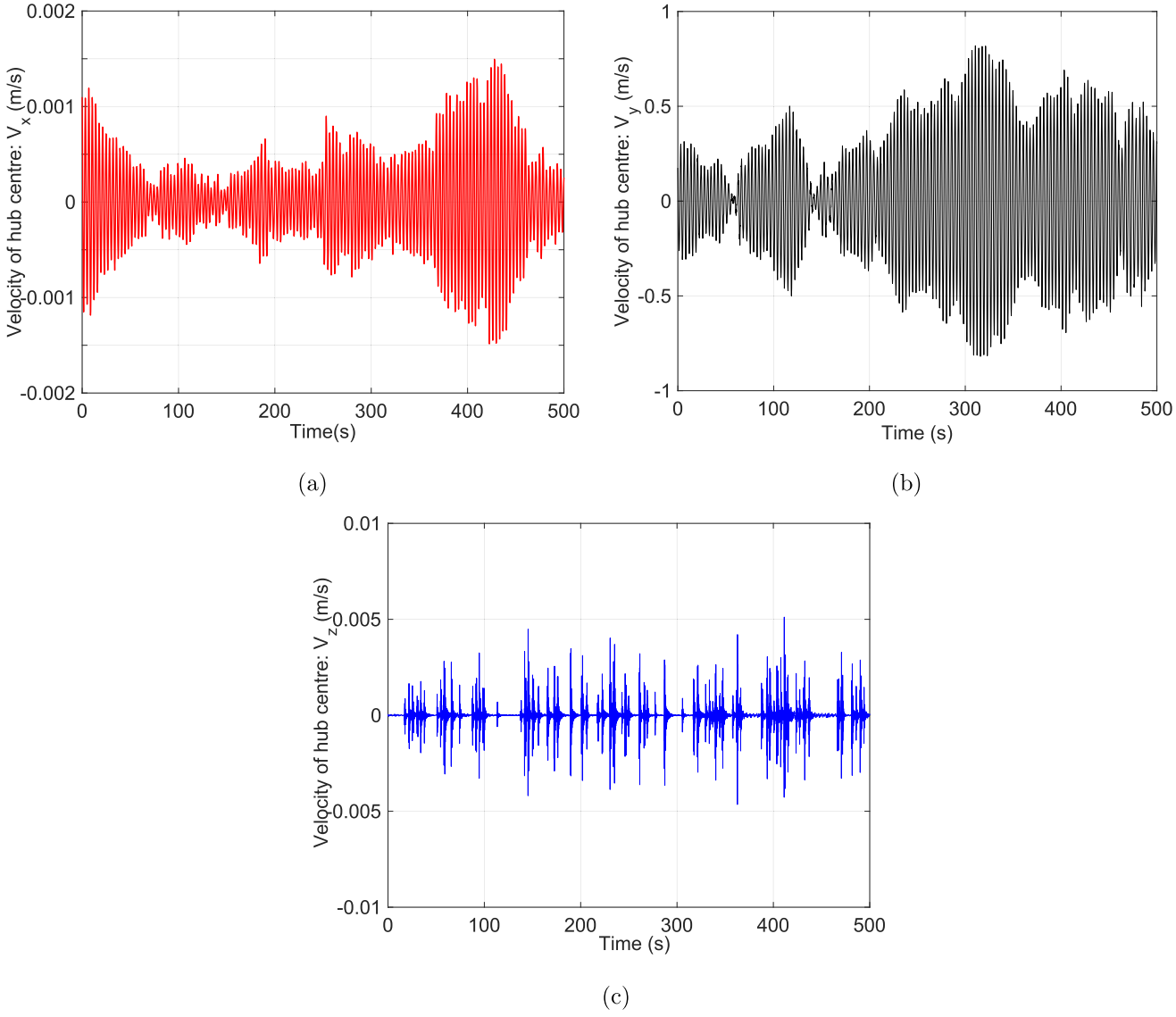

Fig. 12. (a) Velocity of hub centre in the global-X direction (EC-I). (b) Velocity of hub centre in the global-Y direction (EC-I). (c) Velocity of hub centre in the global-Z direction (EC-I).

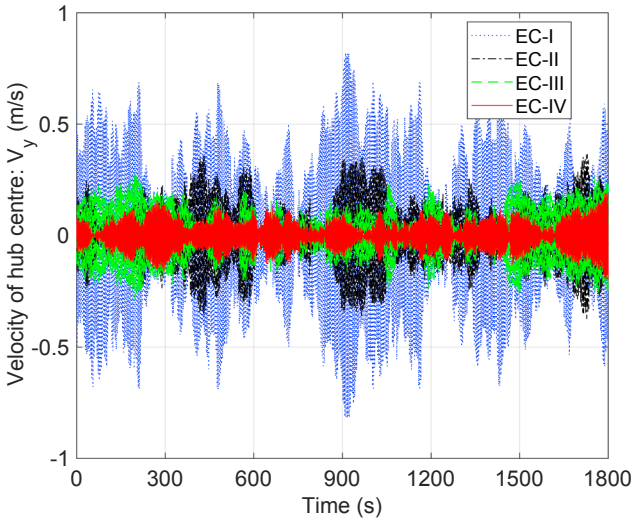

Fig. 13. Comparison of hub motion for all the load cases in the global-Y direction.

centre in the global Y direction for all 4 load cases (EC-I, EC-II, EC-III, and EC-IV), i.e. with $H_s = 2$ m and T_p varying as 4 s, 6 s, 8 s and 10 s, respectively. Load case EC-I exhibits the highest response in the hub of the turbine compared to the other three load cases. This result is because EC-I has a spectral peak period (T_p) of 4 s, which is near the resonance period of the monopile in its first fore-aft mode (4.2 s). Thus, as a result of limited damping, it leads to a very high resonance-driven hub oscillation motion and would be significantly critical for the mating process. In practice, it is very likely to have waves of the same order, and thus, it would be preferable to have an artificial damping system for the monopile. One way to compensate such a motion would be to apply a tuned mass damper system. Such a system could prevent amplification of hub motions during such resonance actions.

5.2. Blade root motions and relative velocity between blade root and the hub

Unlike the hub motions, the blade root motions are affected by the aerodynamic wind forces and tugger line forces that constrain the blade motion. We considered a mean wind speed (U_w) of 10 m/s and corresponding turbulence intensity (T_I) of 0.12 for all the load cases considered in this study. Thus, similar response behaviour in the blade root is observed for all the load cases. Fig. 14(a) presents a comparison of the time histories for the velocities of the blade root in the global X, Y and Z directions for load case EC-I. The velocity of the blade root in the X direction (represented by red curve) is significantly less than the velocities in the Y and Z directions. Hence, the motion of the blade in the X direction is considered to be insignificant for mating operations. Furthermore, the velocities of the blade root in the global Y and Z directions are comparable, although the former has a higher response magnitude. Nevertheless, since the hub motions as discussed are found to be insignificant in the global Z direction, this paper considers the velocity of the blade root in the global Y direction for evaluating the relative velocity.

The relative velocities between the blade root and the hub are evaluated for all the load cases. Fig. 14(b) presents the time histories for two load cases (EC-I and EC-IV), with the former presenting significantly higher values due to a large contribution from the hub motion. This can be confirmed from Table 5, where the magnitude of the relative velocity between the blade root and hub for load case EC-I is reported to be approximately 1.3 m/s compared to EC-IV having a value of 0.63 m/s. The relative velocity also decreases with increasing spectral peak period. Finally, important response statistics such as mean, standard deviation (SD) and extreme value (Max) for hub motions, blade root motions and the relative velocities between them are evaluated based on the average of the five simulations presented in Table 5. Here, the statistical parameter 'Max' for each load case corresponds to the average of 5 seeds, with each seed evaluated for 90% fractile maximum value. The response measure 'Max' obtained for the relative velocity between the root and hub in the global Y direction is utilized as the impact velocity for performing the impact investigation in Abaqus.

5.3. Impact-induced damage assessment at the blade root guiding connection

The impact analyses were considered for a scenario in which the blade root guiding connection during mating suffers sideways impact with the hub. Before the results of the damage assessment on the blade root are presented, the validity of the numerical model's suitability needs to be discussed. Hence, a mesh convergence study for different element sizes considered for the local sub-model and a discussion of the energy output history are presented and discussed first. Since it is assumed in this study that the motion of the hub does not change due to impact with the blade, the displacement and acceleration of the hub with and without the blade impact are also presented. This result would confirm the assumption of utilising the relative velocity between the blade root and hub for the impact investigation. Then, the damages

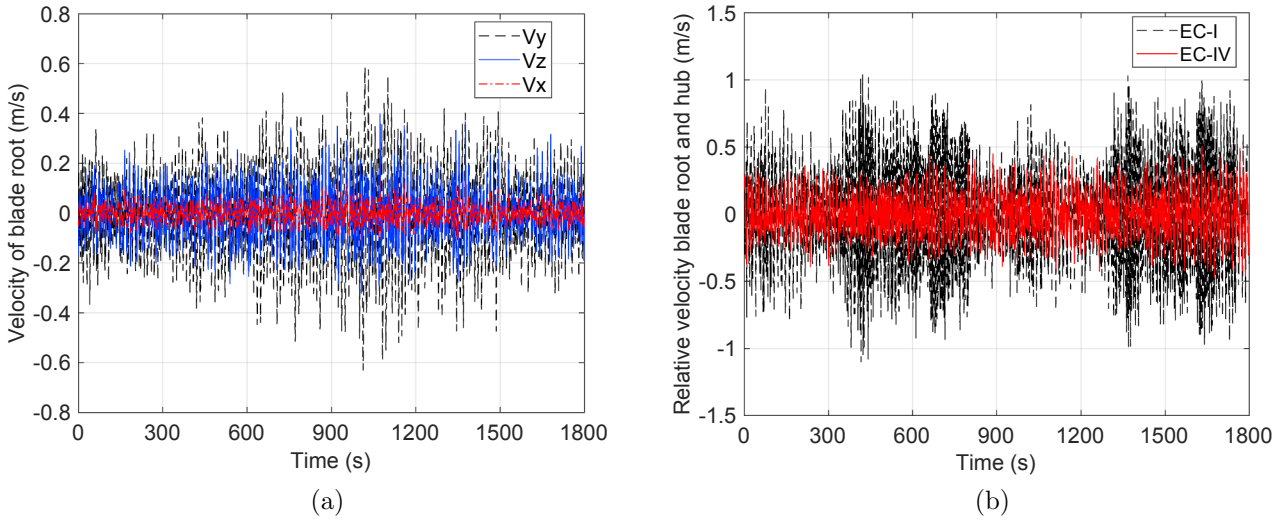

Fig. 14. (a) Velocity of blade root in global X, Y and Z (EC-I). (b) Relative velocity between blade root and hub for EC-I and EC-IV.

Table 5
Response statistics for the load cases.

EC	Velocity of hub (Y)			Velocity of root (Y)			Relative velocity (Y)		
Statistics	Mean	SD	Max	Mean	SD	Max	Mean	SD	Max
EC-I	0.92	0.01	0.99	0.53	0.05	0.59	1.18	0.11	1.30
EC-II	0.54	0.04	0.60	0.56	0.05	0.61	0.83	0.11	0.92
EC-III	0.37	0.04	0.41	0.54	0.06	0.61	0.67	0.07	0.81
EC-IV	0.2	0.02	0.22	0.53	0.05	0.59	0.49	0.06	0.63

occurring at the blade root guiding connection and its components are presented and discussed.

5.3.1. Mesh convergence analysis and energy output examination

A mesh convergence study is performed for the components of the guiding connection, where the consistency of the results with the element sizes used in the local sub-model is investigated. Here, the results are presented for a load case with an impact velocity of 0.81 m/s [EC-III]. The (1) maximum equivalent plastic strain (ϵ_{pl}, represented by PEEQ) developed in the guide pin, (2) through-the-thickness normal strain (ϵ_{33}, represented by LE33) developed around the in-plane hole of the root laminate, and (3) computational time normalised with 3 days of cluster time on a supercomputer are chosen as the controlling parameters. In the convergence analysis, the sizes of the C3D8R brick elements in the bolt and around the in-plane hole of the root laminate are taken as 2.49 mm, 5.56 mm, 8.16 mm and 10.28 mm. Fig. 15(a) shows a comparison of these controlling parameters with varying element sizes, where it can be observed that the element sizes of 5.56 mm and 2.49 mm provide consistent results for both components of the sub-model, with the former taking an analysis time that is 1.8 times faster to solve the numerical problem. Thus, the element size of 5.56 mm is chosen for discretising the sub-model and performing the impact investigation.

After the mesh convergence study, the energy output history results are also examined to validate the model's suitability. This is required especially for a numerical analysis based on an explicit-algorithm-based solver. Fig. 15(b) presents the energy evolution history for a case where the blade root guiding connection impacts the hub with an impact velocity of 0.81 m/s. As shown, the total energy in the system (ETOTAL) is constant throughout the simulation time, with the sum of kinetic energy (ALLKE) and internal energy (ALLIE) corresponding to the total energy (ETOTAL).

This result confirms that the energy conservation principle was satisfied for the impact analysis. Furthermore, the artificial strain energy (ALLAE), which is developed in the numerical analysis to constrain any potential hourglass effects, is found to be significantly small (Fig. 15(b)) (and was less than 2% of the total energy). Overall, these checks validate the numerical suitability of the model utilized in this study.

5.3.2. Contact force history and motion of the hub with and without the blade impact

Fig. 16(a) presents the evolution of the contact-force history along with the evolution of the internal energy developed in the blade due to impact with the hub. It is observed that the internal energy developed in the blade closely follows the contact force history curve. It can also be observed from the contact force curve that the blade root guide pin comes into contact with the hub at approximately 0.04 s of the simulation time, with a maximum contact force of 73 kN developed at almost 0.4 s of the simulation time. This is the maximum time duration where any damage in the blade due to impact is observed. The contact duration from 0.4 s to 0.63 s presents a phase where the blade, due to the eccentricity of its impact, rotates as a rigid body while being in contact with the hub. Finally, the contact of the guide pin with hub lasts until 0.63 s of the simulation time, and the blade separates from the hub. This contact force history is then taken as an input to an external force DLL (dynamic link library) in HAWC2. This is to check the blade impact on the overall hub motion.

Fig. 16(b) and (c) compare the displacement and acceleration in the hub with and without the blade impact. As shown, the effect of the blade impact on the motion of the hub is very small. This result is expected because the mass of the hub is almost 10 times the mass of the blade, and the compliance of the guide pin does not influence the global behaviour of the hub. This confirms our assumption about the use of the relative velocity between the blade root and hub for impact investigation.

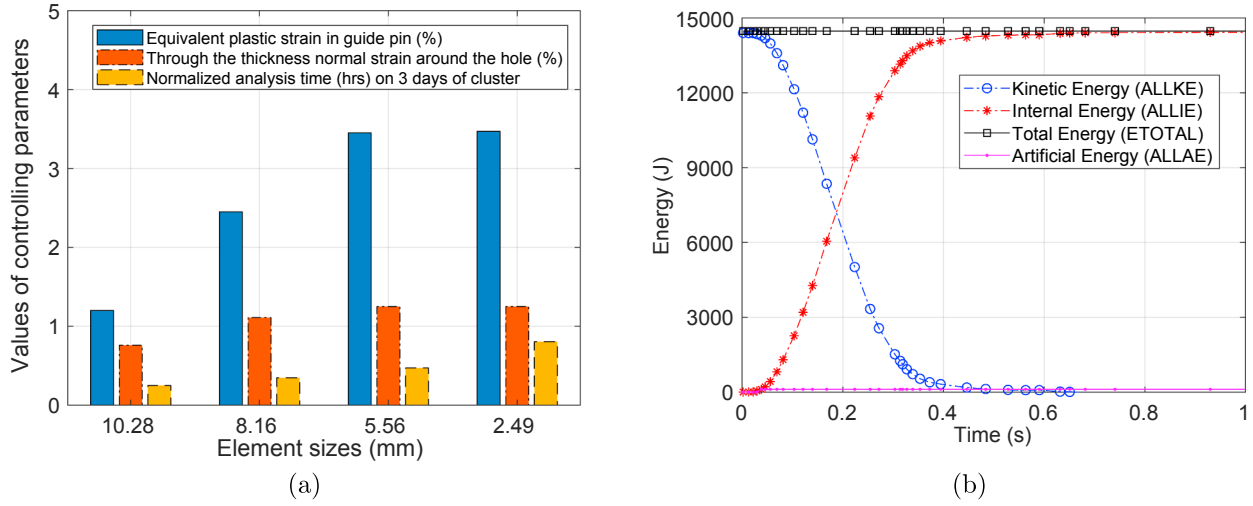

Fig. 15. (a) Mesh convergence study (V_x = 0.81 m/s). (b) Energy evolution history (V_x = 0.81 m/s).

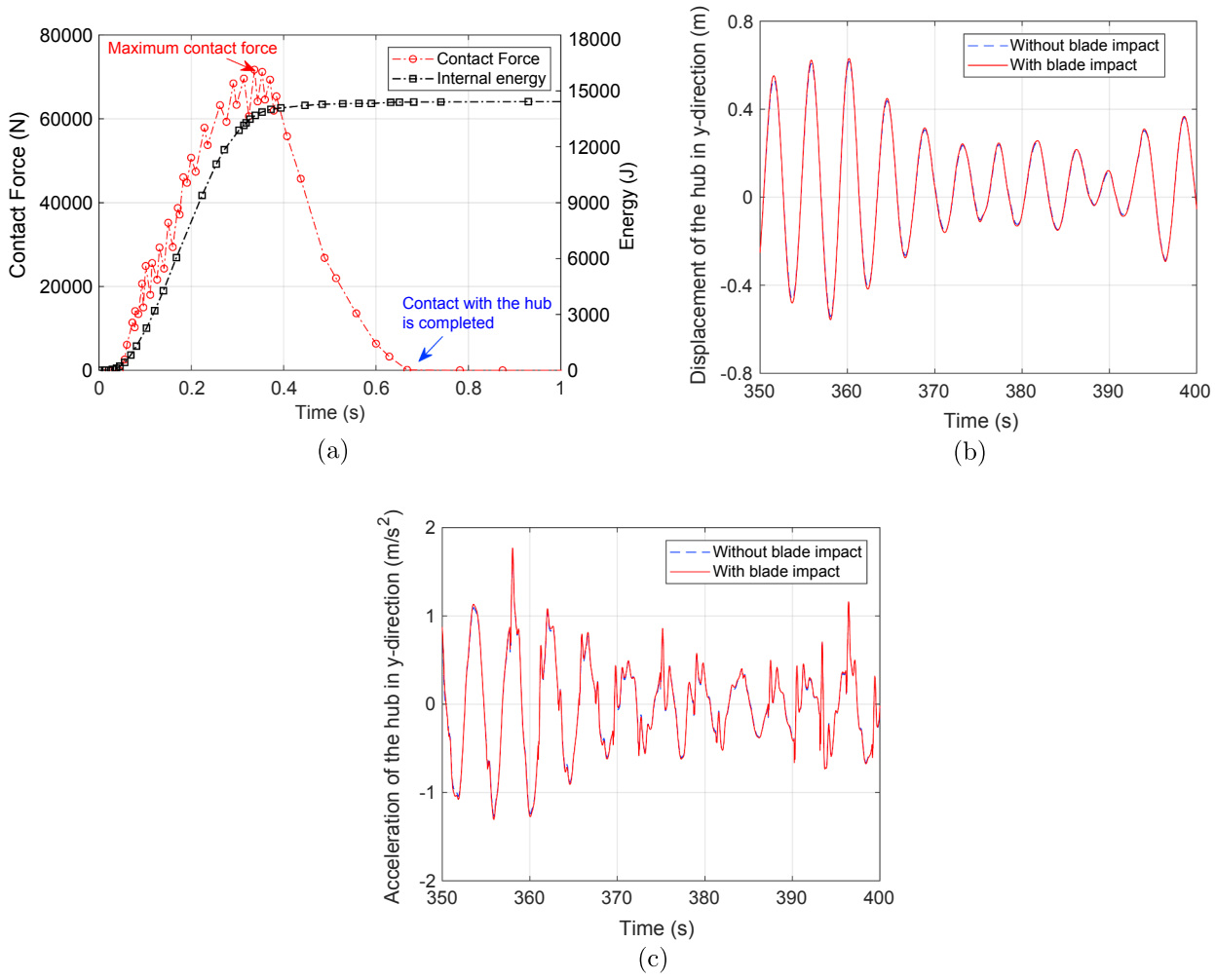

Fig. 16. (a) Contact force history with internal energy evolution. (b) Displacement of the hub. (c) Acceleration of the hub.

5.3.3. Damage assessment of the blade root and its consequence on installation tasks

Fig. 17 presents the initial (t = 0 s) and final deformation states (t = 1 s) of the blade root (shown in grey colour) for a case where its guide pin (shown in blue colour) impacts the hub (illustrated by green colour) with an impact velocity of 1.30 m/s [EC-I].

As shown, due to the impact, there is a permanent deformation and bending of the guide pin bolt (Fig. 17). This can be further confirmed from Fig. 18, where the final strain state of the local sub-model consisting of root laminate, guide pin and barrel nut is magnified and presented. It can clearly be observed that there is a substantial development of plastic strain (PEEQ) in the guide pin, closer to the region where it meets the root laminate and the barrel nut.

This leads to significant plastic deformation in the guide pin and is characterised by the pin bolt being permanently bent to an angle of approximately 15^0 (Fig. 18) from the initial state. From an installation

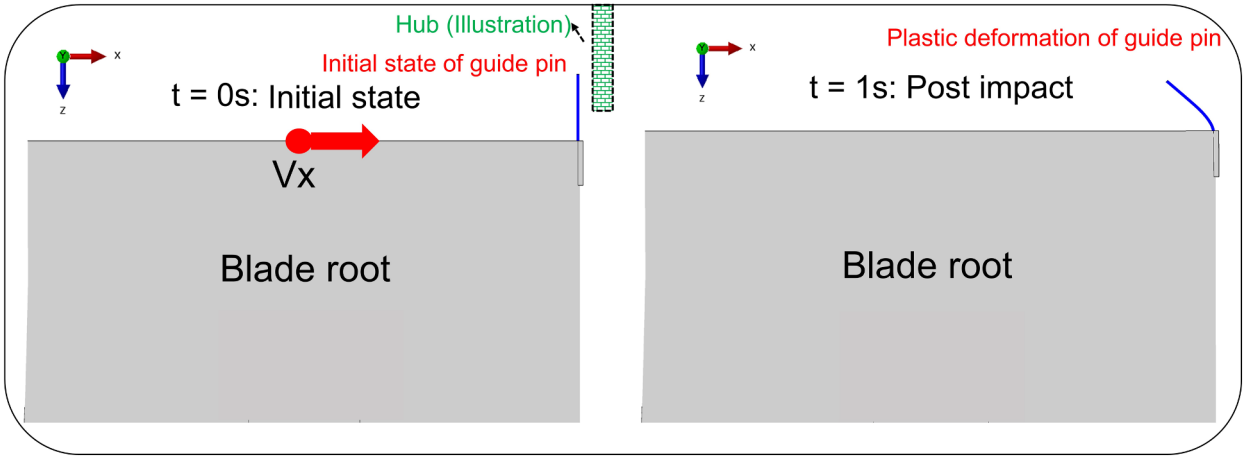

Fig. 17. Pre and post impact deformation state of the blade root connection (V_x = 1.30 m/s).

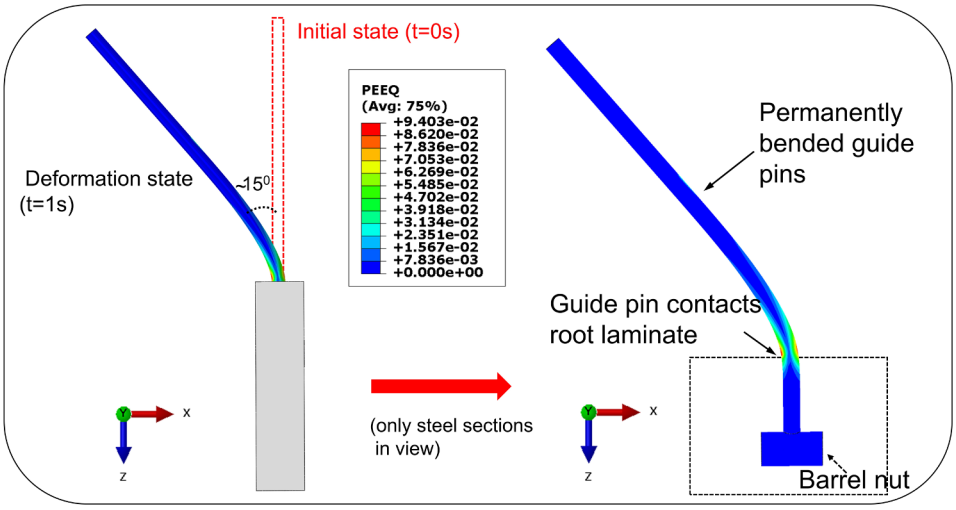

Fig. 18. Plastic deformation and bending of guide pins due to impact (V_x = 1.30 m/s).

perspective, this bending of the guide pin bolt would mean that in cases of an accidental impact during mating, the lifted blade would not be mated and would require being hoisted back onto the deck of the vessel with this damaged guide pin bolt requiring replacement. This would indeed lead to installation delays and increase the overall installation cost. Nevertheless, the bending of the guide pin exclusively is not considered as a critical failure mode for the blade's structural integrity because these bolts can still be replaced with newer ones and the blade is considered again for another mating trial. Additionally, as a result of such an impact, no plastic strain develops in the barrel nut, inferring a sound barrel nut before and after the impact. This is a good indicator from an installation perspective as the barrel nut is permanently attached in the blade root by an adhesive connection and, in the case of any damage, cannot be replaced with a newer one.

Furthermore, due to bending of the guide pin bolt during and after the impact, an impact occurs between the guide pin and the root laminate around the in-plane hole, which could possibly damage the adjoining laminates. Fig. 19 shows the cross-sectional cut view of the sub-model, where at t = 0 s (initial state), it can be observed that there is no contact between the guide pin and the laminate initially. This is because in the finite element model of the guiding connection, the nominal diameter of the guide pin was kept smaller than the in-plane hole diameter at the root laminate. However, at t = 1 s, as a result of the bending of the guide pin, contact between them could clearly be observed around the head region of the in-plane hole (Fig. 19). Since the contact interaction properties were already defined between these components in the finite element model, any possible failure occurring in the laminate due to such impact forces could be predicted based on the stress criterion implemented and are hence discussed here.

The impact-induced stresses developed in the laminate around the in-plane hole are investigated, and the failure index with normalised stress exposure factors for all the stress states are analysed. First, the in-plane stress states in the laminate are checked with their allowable values. It is found that the in-plane normal (σ_{11} and σ_{22}) and in-plane shear stresses (σ_{12}) are below their allowable values, implying that their normalised exposure factors in the laminate are below the failure threshold values. However, the through-the-thickness transverse normal stress (σ_{33}) and inter-laminar shear stresses (σ_{13}, σ_{23}) in the laminate are found to be critical and thus further reported and discussed here. This observation is consistent with the behaviour of the composite laminates whose strength in the transverse direction is significantly lower than the strength and stiffness in its in-plane direction.

Fig. 20 presents the impact-induced stress exposure factors for the through-the-thickness normal (σ_{33}) and inter-laminar shear stresses (σ_{13} and σ_{23}) developed in the laminate around the in-plane hole. These exposure factors are denoted by the parameter failure index (F_I) defined

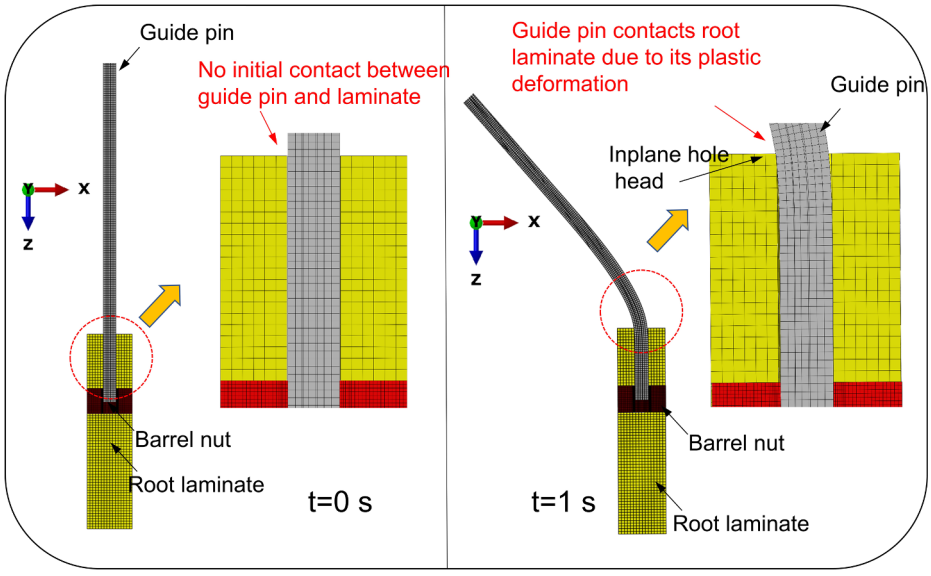

Fig. 19. Contact of the guide pin with the laminate.

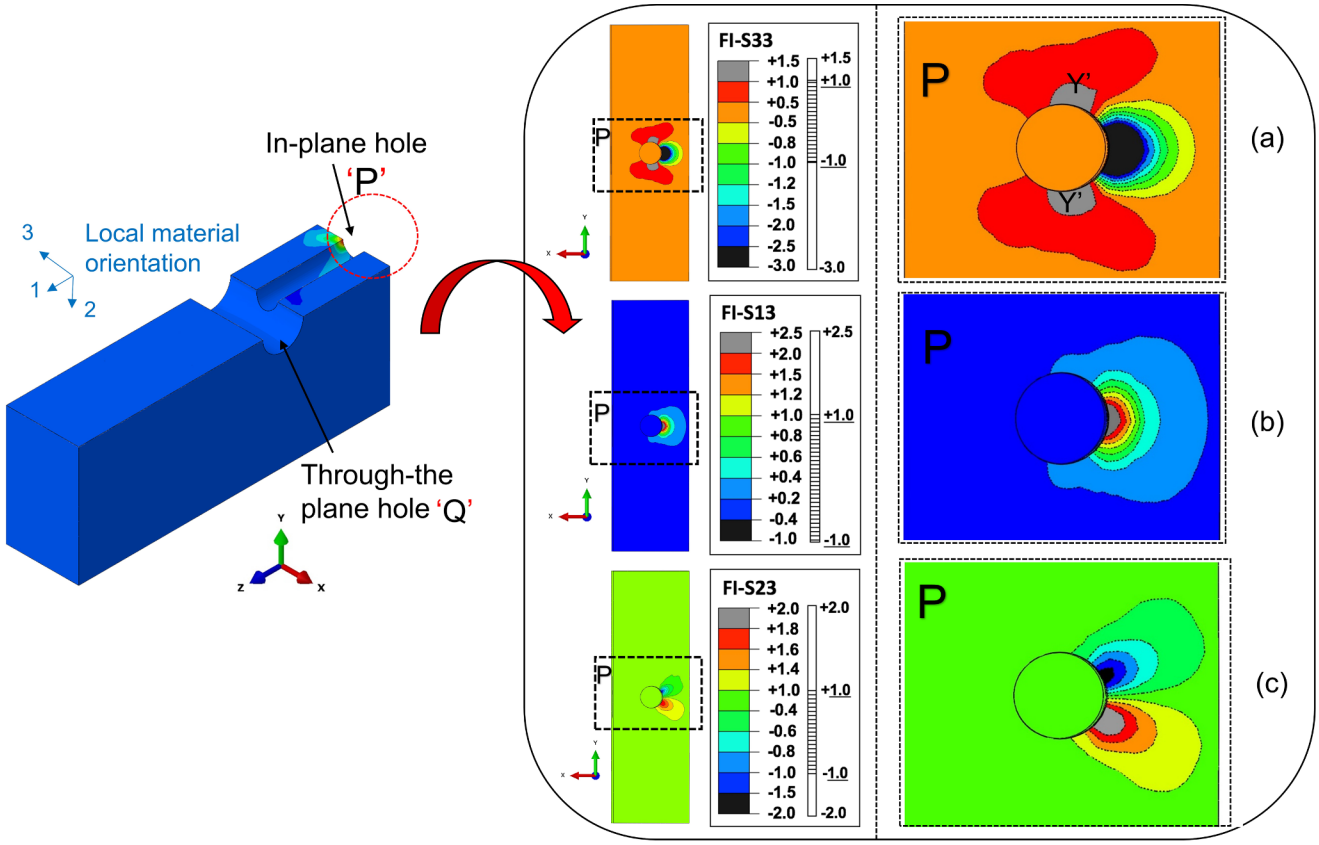

Fig. 20. Failure Index representing stress exposure factors for S33, S13 and S23 (EC-I).

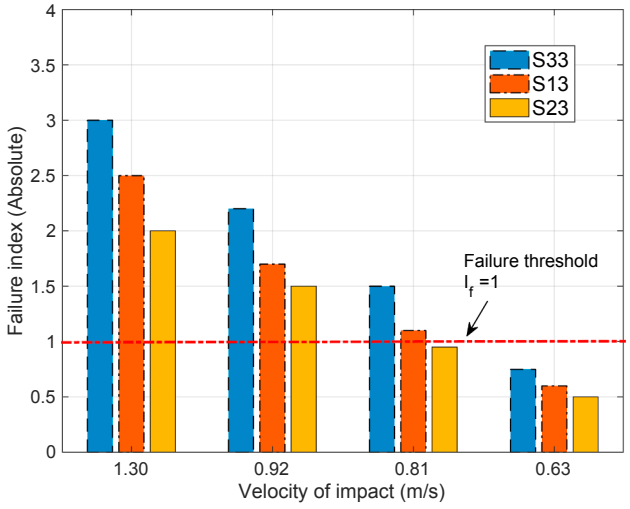

Fig. 21. Failure index in the root laminate for all the load cases.

for the corresponding stress state as $F_I(S_{33})$, $F_I(S_{13})$ and $F_I(S_{23})$. Here, any exposure factor lying between 1 and -1 ($-1 < F_I(S_{ij}) < +1$) suggests that the stresses in the region of the laminate lie below the allowable stresses (i, j) and thus have not failed. This range of exposure factors ($\forall : F_I \in (-1, 1)$) is also explicitly marked with hashed lines in the legends of the contour plot in Fig. 20 for clarity. Again, any region with exposure factors lying outside this range ($\forall : F_I(S_{ij}) \in (-\infty, -1] \cup [+1, \infty]$) predicts the occurrence of failure in the laminate. As shown in Fig. 20, the regions around the in-plane hole of the root laminate have exposure factors greater than 1 in all three stress states (σ_{33}, σ_{13}, σ_{23}), implying failure in the laminate. Moreover, an exposure factor of $+1.5$ in $F_I(S_{33})$ (Fig. 20(a)), which corresponds to tensile through-the-thickness normal stresses (shown in grey colour), developed in the transverse direction of the in-plane hole (Y′Y′) is a very critical failure stress state. This is due to the orientation of the plies, which are stacked in the transverse direction in these regions and are highly likely to lead to delamination cracks in the Mode I crack-opening fracture mode. These delamination cracks could negatively affect the blade's structural integrity because these in-plane holes are subjected to compressive stresses during the normal operational loads. This could lead to crack growth in these regions if the damage levels are not analysed due to such impacts and the crew decides to install the blades onto the hub. Thus, in the case of such damages, it would require major repair works at the root when the blade is brought back onto the vessel. There is also a high probability that the blade had developed critical damages and is declared to be unfit from a structural perspective and hence rejected. This would lead to failure of the blade installation process, leading to heavy losses. Thus, such a failure mode is not acceptable from the perspective of the blade's structural integrity, and any environmental load case causing such damage at the root laminate in the mating phase must be avoided. Nevertheless, the extent of cracks and a fracture-mechanics-based delamination approach would require further investigation and will be considered in future work. However, based on the criterion implemented for the laminate, this study suggests that for load case EC-I, the laminate has failed.

Fig. 21 summarises the failure index evaluated for the through-the-thickness normal and transverse shear stresses developed at the root laminate for all the load cases considered in this paper. It can clearly be observed that for all the load cases, except for EC-IV, the laminates have a failure index exceeding 1, suggesting failure in the laminates. This would mean that the mating operations of the blade root with the hub must be avoided in such sea states [Cases I, II, and III] as there could be high consequences on the blade's structural integrity upon its impact, given failure predicted in the laminates. Additionally, for all the load cases considered in this paper, the guide pin bolt suffers permanent

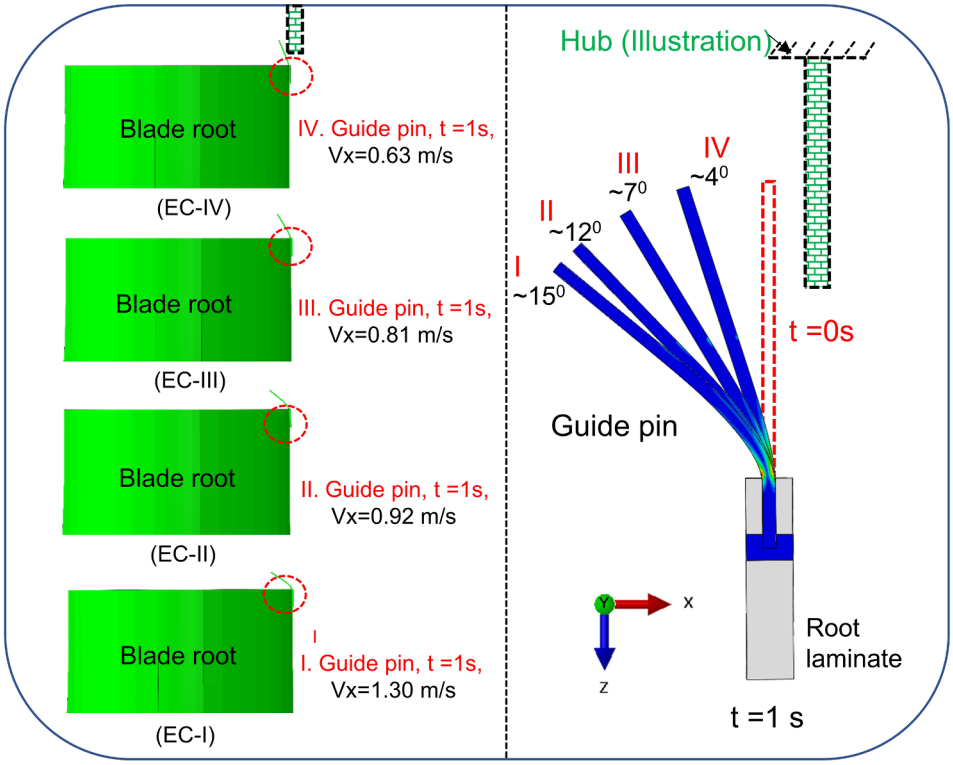

Fig. 22. Plastic deformation in the guide pin for all the load cases.

deformation and bends (Fig. 22). Thus, the blade would be required to be hoisted back onto the vessel deck for all the cases, and the guide pin would be required to be replaced with a newer one. However, for load case EC-IV, since the guide pin had bent at an angle of 4^0 and there were no damages in the laminates, the blade can be lifted again, and another mating trial can be performed as soon as the newer bolts are reinstated.

5.3.4. Summary of the damages and the consequence on the installation activities

Table 6 illustrates the damages, post-impact consequences and planning chart for the mating operation between the blade and the hub considering impact risks. It can be observed that for all the cases due to guide pins becoming damaged, the blade would need to be brought back onto the vessel and would require repair of the blade root by replacing the damaged guide pin with a newer one. However, it is only for load case EC-IV could the blade be lifted for another trial after the replacement of guide pins with newer bolts. For the other load cases, since there is damage of the root laminate, which could develop delamination cracks, it would require further investigation and checks on the vessel before the blade is either given another mating trial, repaired or rejected. In either case, it would lead to severe installation delays and

Table 6
Damage, post-impact consequences and planning chart.

EC	Damages in the guiding connection			Post-impact consequences and crew decision				Planning
Variables	Guide Pin	Barrel Nut	Root laminate	Blade back on vessel	Repair	Another Trial	Further check	Sea States
EC I	D	ND	D	Y	Y	NP	R	NA
EC II	D	ND	D	Y	Y	NP	R	NA
EC III	D	ND	D	Y	Y	NP	R	NA
EC IV	D	ND	ND	Y	Y	P	NR	A

Keywords: **D**-*Damaged*; **ND**-*Not Damaged*; **Y**-*Yes*; **N**-No; **NP**-*Not possible*; **P**-*Possible*; **R**-*Required*; **NR**- *Not Required*; **NA**-*Not acceptable*; **A**-*Acceptable*

Keywords: **D**-*Damaged*; **ND**-*Not Damaged*; **Y**-*Yes*; **N**-No; **NP**-*Not possible*; **P**-*Possible*; **R**-*Required*; **NR**- *Not Required*; **NA**-*Not acceptable*; **A**-*Acceptable*

critical structural damages, and it is thus preferable to accept only EC-IV as an acceptable sea state out of all the sea states considered in this study. Such an approach with damage, consequences and planning chart could be utilised in the future to elaborately consider the impact risks for all possible sea states and evaluate response-based operational limits considering structural damage criteria.

6. Concluding remarks

This study addresses the final stage of the mating process of the blade root with the hub, which is highly challenging and requires high precision. It is discussed that due to the relative motions manifested during the alignment phase, an impact could occur between the blade root and the hub when the guiding connection is being positioned. Here, the sideways impact of a guiding connection at the blade root with the hub is investigated. For this purpose, the global installation system representing the mating operation is modelled in the HAWC2 code. Four different environmental load cases are considered, which represented the mating operation in a relatively rough sea state and with collinear wind and wave conditions. Dynamic response analyses for all the load cases are performed, and response statistics including impact velocities are evaluated. The guiding connection, as a local sub-model for the DTU 10 MW blade, is separately modelled using finite element modelling in Abaqus and is coupled with the blade at its root with shell solid coupling feature. Finally, the impact analyses are considered with the hub for four different impact velocities, each corresponding to a specific environmental load case. The major conclusions from the study are as follows:

- The blade root motions and the hub motions during the mating phase are critical, with the dominant contribution to the relative velocity coming from the latter. The hub motions are quite sensitive to the spectral peak period of the waves. The maximum responses in the hub are obtained for the load case for the sea state with $T_p = 4$ s [EC-I]. This approaches the natural period of the monopile in the first aft mode, and it contributes to the highest relative velocity manifested between the blade root and hub.
- The relative motion evaluated for collinear wave and wind conditions inferred the occurrence of a sideways impact of the blade root with the hub as the critical impact event. From a structural perspective, this scenario is susceptible to large damages given the impact in the transverse direction of the bolt connections.
- The guiding connection is modelled in Abaqus, and the root laminate is defined with a homogenised triaxial layup of $[0/+45/-45]$, with properties derived based on the homogenisation principle. This study considers the finite element analysis based on an explicit algorithm. The von Mises with isotropic hardening model and equivalent plastic strain criterion are utilised for predicting any failure in the steel bolt, whereas a maximum stress criterion is considered for predicting any failure in the composite root laminate. Failure indices are also formulated in the maximum stress criterion, which present normalised exposure factors for the stress states. Numerical validity based on the mesh convergence study and energy output history examination for the explicit-based finite element analysis are checked, and the numerical models utilised for the impact investigation are found to be suitable.
- It is further found that due to impact, for all the load cases, there are severe bending and plastic deformations of the guide pin. Consequently, this causes the contact of the guide pin with the laminate near its in-plane hole. The stresses around the in-plane hole are checked. The through-the-thickness normal stresses and transverse shear stresses for all the load cases, except for EC-IV, exceeded their allowable values, which suggests failure in the laminates.
- For all the load cases and damages in the components, consequences to the overall installation task and crew decisions to repair, replace or continue with another mating trial are discussed. It is noted that any damage to the guide pin bolts (a damage mode that was obtained for all the load cases) would require the blade to be hoisted back onto the vessel and would cause installation delays. However, a case with only guide pins being damaged is not a critical failure mode, as these can be replaced with newer ones and the blade could be lifted for another mating trial. It is further discussed that any damage to the laminates during such impact could lead to the progression of delamination cracks in Mode I crack-opening fracture mode and would be critical for the blade's structural integrity, requiring a further check. Thus, if such damage modes occur, the blade cannot continue with another trial after the impact. This could lead to installation delays and loss of favourable weather windows, and thus, from a conservative approach, it is recommended to not allow any damages in the blade laminate at the root during impact. Thus, for all the load cases considered in this study, only EC-IV is found to be an acceptable sea state for the mating operation from structural damage criteria.

7. Limitation and future work

In the current work, the impact assessment of wind turbine blade root during an offshore mating process was investigated. Certain assumptions and simplifications were made during the numerical modelling. The jack-up crane vessel was not modelled in multi-body simulations, and the crane tip was considered rigidly fixed. However, the jack-up crane vessel's motion can have eigen period in the range of 0.4–3 s [49], and can have wave-induced crane tip motions particularly in short waves. Further, depending on the distance between the jack-up legs and the monopile, the presence of jack-up crane vessels during installation may have diffraction effects on the wave loads applied on the monopile. It is interesting to investigate such effects in future. Also, for defining the monopile-soil interaction, only $p - y$ curve was considered in the study, as the horizontal resistance of the soil govern the critical responses in the hub. The $t - z$ and $q - z$ curves which describes the soil-skin friction and end-bearing resistance of the soil respectively will have limited effect and were not included in the study. However, for practical offshore installation sites, soil surveys are thoroughly conducted and $t - z$ and $q - z$ curves are also available for design purposes. Therefore, it is interesting to include these curves in the numerical model and investigate the dynamic responses of the system. Finally, in the finite element analysis, the damage assessment results were investigated on a homogenised root laminate. However, in the future, a progressive failure analysis with emphasis on delamination modelling must be considered.

Acknowledgement

This work was made possible through the SFI MOVE projects supported by the Research Council of Norway, NFR project number 237929. The authors would also like to thank the anonymous reviewer for thoughtful comments and suggestions.

References

[1] Li L, Gao Z, Moan T. Operability analysis of monopile lowering operation using different numerical approaches. International Society of Offshore and Polar Engineers (ISOPE); 2016.
[2] Verma AS, Vedvik NP, Gao Z. Numerical assessment of wind turbine blade damage due to contact/impact with tower during installation. IOP conference series: materials science and engineering, vol. 276. IOP Publishing; 2017. p. 012–25.
[3] Pineda I, Tardieu P. The european offshore wind industry – key trends and statistics; 2016. <https://windeurope.org/about-wind/statistics/offshore/european-offshore-wind-industry-key-trends-and-statistics-2016/> [accessed: -06-01].
[4] Wind Europe. The European offshore wind industry–key trends and statistics; 2017. Technical report.
[5] Corbetta G, Mbistrova A, Ho A, Guillet J, Pineda I. The European offshore wind industry–key trends and statistics 2013. Eur Wind Energy Assoc 2014:4–13.
[6] Groot DK. A novel method for installing offshore wind turbine blades with a floating vessel. Master thesis, TU Delft; 2015.

[7] Verma AS, Haselbach PU, Vedvik NP, Gao Z. A Global-local damage assessment methodology for impact damage on offshore wind turbine blades during lifting operations. ASME 2018 37th International Conference on Ocean, Offshore and Arctic Engineering. American Society of Mechanical Engineers; 2018. V010T09A064–V010T09A064.

[8] Darius S. GE unveils market–changing 12MW offshore wind turbine. <http://www.rechargenews.com/wind/1443296/ge-unveils-market-changing-12mw-offshore-wind-turbine> [accessed: 2018-03-01].

[9] Verma AS, Zhao Y, Vedvik NP, Gao Z. Explicit structural response-based methodology for assessment of operational limits for single blade installation for offshore wind turbines. In: 4th ICOE2018, Springer Publications.

[10] Toft HS, Branner K, Berring P, Sørensen JD. Defect distribution and reliability assessment of wind turbine blades. Eng Struct 2011;33(1):171–80.

[11] Verma AS, Vedvik NP, Gao Z. A comprehensive numerical investigation of the impact behaviour of an offshore wind turbine blade due to impact loads during installation. Ocean Eng 2018. [Revision submitted].

[12] Jiang Z. The impact of a passive tuned mass damper on offshore single-blade installation. J Wind Eng Indus Aerodynam 2018;176:65–77.

[13] https://www.power-technology.com/projects/lake-winds-energy-mason-county-michigan/attachment/lake-winds-energy-mason-countymichigan6/, Picture.

[14] Jiang Z, Gao Z, Ren Y, Li Zhengru, Lei D. A parametric study on the blade final installation process for monopile wind turbines under rough environmental conditions. Eng Struct 2018;172(201):1042–56.

[15] Van Buren Eric. Private communication with Eric Van Buren, Fred. Olsen Windcarrier [accessed: April 18, 2018].

[16] Habali S, Saleh I. Local design, testing and manufacturing of small mixed airfoil wind turbine blades of glass fiber reinforced plastics: part I: design of the blade and root. Energy Convers Manage 2000;41(3):249–80.

[17] Peeters M, Santo G, Degroote J, Paepegem WV. The concept of segmented wind turbine blades: a review. Energies 2017;10(8):1112.

[18] Brøndsted P, Nijssen RP. Advances in wind turbine blade design and materials. Elsevier; 2013.

[19] Ketele S. Detailed modeling of connections in large composite wind turbine blades. Master's thesis, Universiteit Gent; 2013.

[20] Martínez V, Güemes A, Trias D, Blanco N. Numerical and experimental analysis of stresses and failure in t-bolt joints. Compos Struct 2011;93(10):2636–45.

[21] Briggs AJA, Zhang ZY, Dhakal HN. Study on T-bolt and pin-loaded bearing strengths and damage accumulation in E-glass/epoxy blade applications. J Compos Mater 2015;49(9):1047–56.

[22] Eriksen BM. Wind and tidal turbine blade root connection. Master's thesis, Norwegian University of Science and Technology (NTNU), Trondheim; 2011.

[23] Mollà IG. Installing a blade in a wind turbine and wind turbines. US Patent App. 14/657,307 (Oct. 1; 2015).

[24] Larsen TJ, Hansen AM. How 2 HAWC2, the user's manual. Tech rep, Risø National Laboratory; 2007.

[25] Kuijken L. Single blade installation for large wind turbines in extreme wind conditions. Master Thesis, Technical University of Denmark; 2015.

[26] Velarde J. Design of monopile foundations to support the DTU 10 MW offshore wind turbine. Master thesis, Norwegian University of Science and Technology (NTNU), Trondheim; 2016.

[27] Damgaard M, Ibsen LB, Andersen LV, Andersen JK. Cross-wind modal properties of offshore wind turbines identified by full scale testing. J Wind Eng Indus Aerodynam 2013;116:94–108.

[28] Shirzadeh R, Devriendt C, Bidakhvidi MA, Guillaume P. Experimental and computational damping estimation of an offshore wind turbine on a monopile foundation. J Wind Eng Indus Aerodynam 2013;120:96–106.

[29] Bak C, Zahle F, Bitsche R, Kim T, Yde A, Henriksen LC, et al. Description of the DTU 10 MW reference Wind Turbine. Progress report Report-I-0092, DTU Wind Energy; 2013.

[30] Faltinsen O. Sea loads on ships and offshore structures. Cambridge university press; 1993.

[31] Morison J, Johnson J, Schaaf S, et al. The force exerted by surface waves on piles. J Petrol Technol 1950;2(05):149–54.

[32] Norge, Standard. NORSOK-N003: actions and actions effects; 2007.

[33] Mann J. The spatial structure of neutral atmospheric surface-layer turbulence. J Fluid Mech 1994;273:141–68.

[34] Hoerner SF. Fluid-dynamic drag: practical information on aerodynamic drag and hydrodynamic resistance. NJ, USA: Hoerner Fluid Dynamics Midland Park; 1965.

[35] International Electrotechnical Comission, IEC 61400-1 Wind Turbine Part 1: Design Requirements. 3rd ed. ed., Geneva, Switzerland; 2007.

[36] Hasselmann K. Measurements of wind wave growth and swell decay during the joint north sea wave project (jonswap). Deutschen Hydrografischen Zeitschrift 1973;8:95.

[37] <https://www.ineffableisland.com/2012/10/wow-worlds-largest-wind-turbineblade.html>, Picture.

[38] Hibbitt H, Karlsson B, Sorensen B. Abaqus analysis user's manual version; 2016.

[39] Tanlak N, Sonmez F, Talay E. Detailed and simplified models of bolted joints under impact loading. J Strain Anal Eng Des 2011;46(3):213–25.

[40] Chou J-S, Ou Y-C, Lin K-Y, Wang Z-J. Structural failure simulation of onshore wind turbines impacted by strong winds. Eng Struct 2018;162:257–69.

[41] Haselbach P, Bitsche R, Branner K. The effect of delaminations on local buckling in wind turbine blades. Renew Energy 2016;85:295–305.

[42] Tavakoldavani K. Composite materials equivalent properties in lamina, laminate, and structure levels. Master's thesis, The University of Texas at Arlington; 2014.

[43] Tørnqvist R. Design of crashworthy ship strutcures. PhD Thesis, Kongens Lyngby, Technical University of Denmark; 2003.

[44] Ehlers S. A procedure to optimize ship side structures for crashworthiness. Proc Inst Mech Eng, Part M: J Eng Marit Environ 2010;224(1):1–11.

[45] Perillo G, Jørgensen J. Numerical/experimental study of the impact and compression after impact on gfrp composite for wind/marine applications. Proc Eng 2016;167:129–37.

[46] Perillo G, Vedivik N, Echtermeyer N. Numerical and experimental investigation of impact on filament wound glass reinforced epoxy pipe. J. Compos. Mater., vol. 49.

[47] Camanho PP. Failure criteria for fibre-reinforced polymer composites. Secção de Mecânica Aplicada, Departamento de Engenharia Mecânica e Gestão Industrial, Faculdade de Engenharia da Universidade do Porto; 2002.

[48] Hu Y, Yang B, Nie SD, Da GX. Performance of high strength structural bolts in tension: effects of tolerance classes. In: International conference on performance-based and life-cycle structural engineering, School of Civil Engineering, The University of Queensland; 2015. p. 776–81.

[49] Zhao Y, Cheng Z, Sandvik PC, Gao Z, Moan T, Van Buren E. Numerical modeling and analysis of the dynamic motion response of an offshore wind turbine blade during installation by a jack-up crane vessel. Ocean Eng 2018;165:353–64.